

D R E A D

DEEP REGOLITH EXPLORATION OF DEIMOS

Team Members: John Courtney, Ben Jensrud, Noe Lepez, Carnell Lyon, Greg McDonald, Keshav Ramanathan,
Justin Shiao, Stacey Tian, Anonto Zaman

Georgia Institute of Technology

AE4342 - Fall 2021

December 2nd, 2021

Fact Sheet

DREAD

DEEP REGOLITH EXPLORATION OF DEIMOS



SCIENCE

OBJECTIVES:

- Determine Deimos' origin.
- Determine Deimos' composition.
- Investigate processes occurring on Deimos' surface.
- Understand whether Deimos is safe for human presence.
- Determine if materials on Deimos could serve as in-situ resources for future human exploration missions.

POTENTIAL PROCESSES:

Weathering:

Causes the asteroid's surface to darken over long periods of time.



Creep:

Regolith piles up around the asteroid's equator.



POTENTIAL RESOURCES:

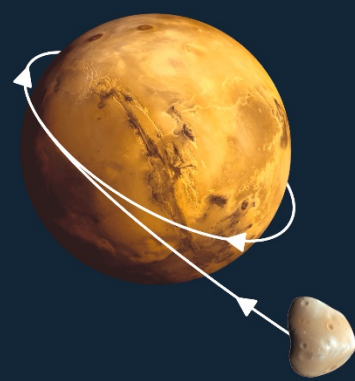
- Carbonate and silicate minerals
- Water or hydroxyl compounds
- Organic compounds
- Martian soil

Resources could be used as fuel for future missions or kept for human consumption. The presence of Martian soil or silicate would hint at which theory of Deimos' origin is correct.

THEORIES OF DEIMOS' ORIGIN:

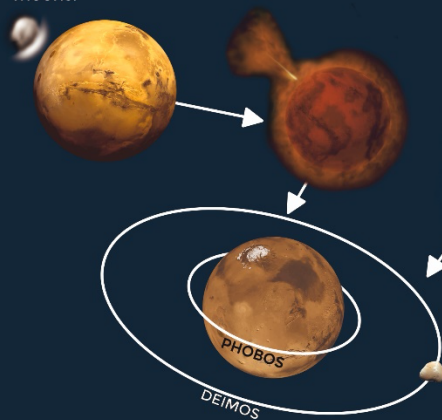
1. Asteroid capture:

Asteroid passes close to Mars and enters Martian orbit.



2. Reaccretion from Mars ejecta

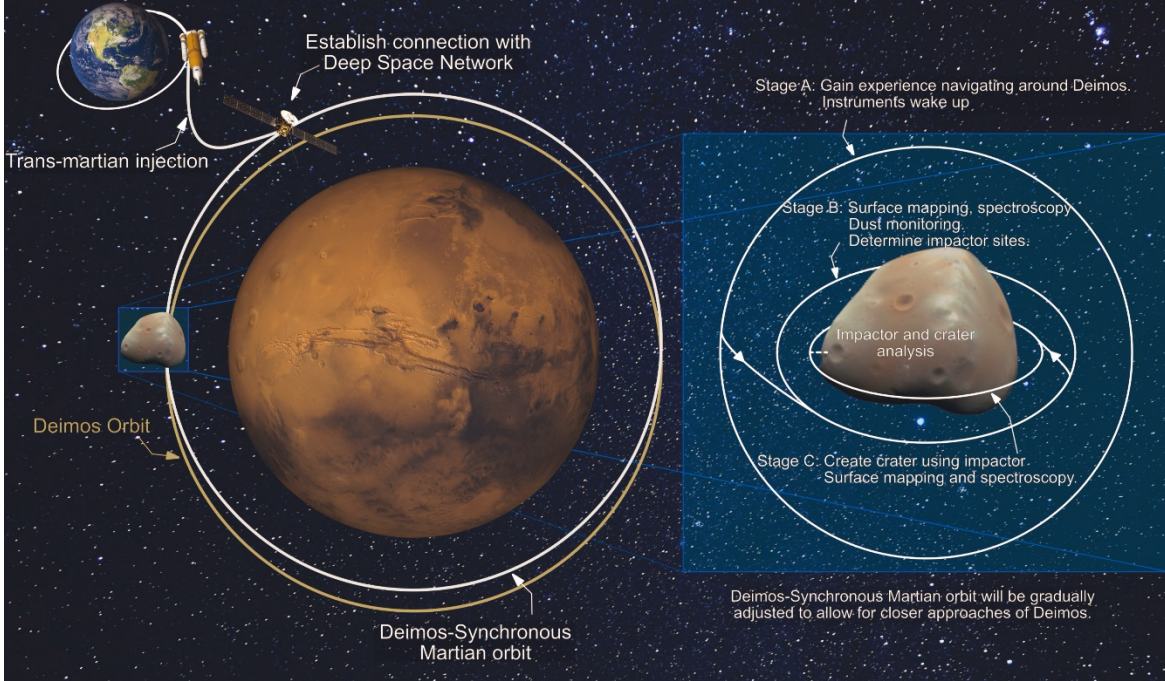
Large asteroid crashes into Mars, sending ejecta into Mars orbit. Ejecta slowly accretes to form martian moons.



3. Mars accretion theory

Martian moons formed at the same time as Mars, from the same dust cloud.

MISSION CONCEPT



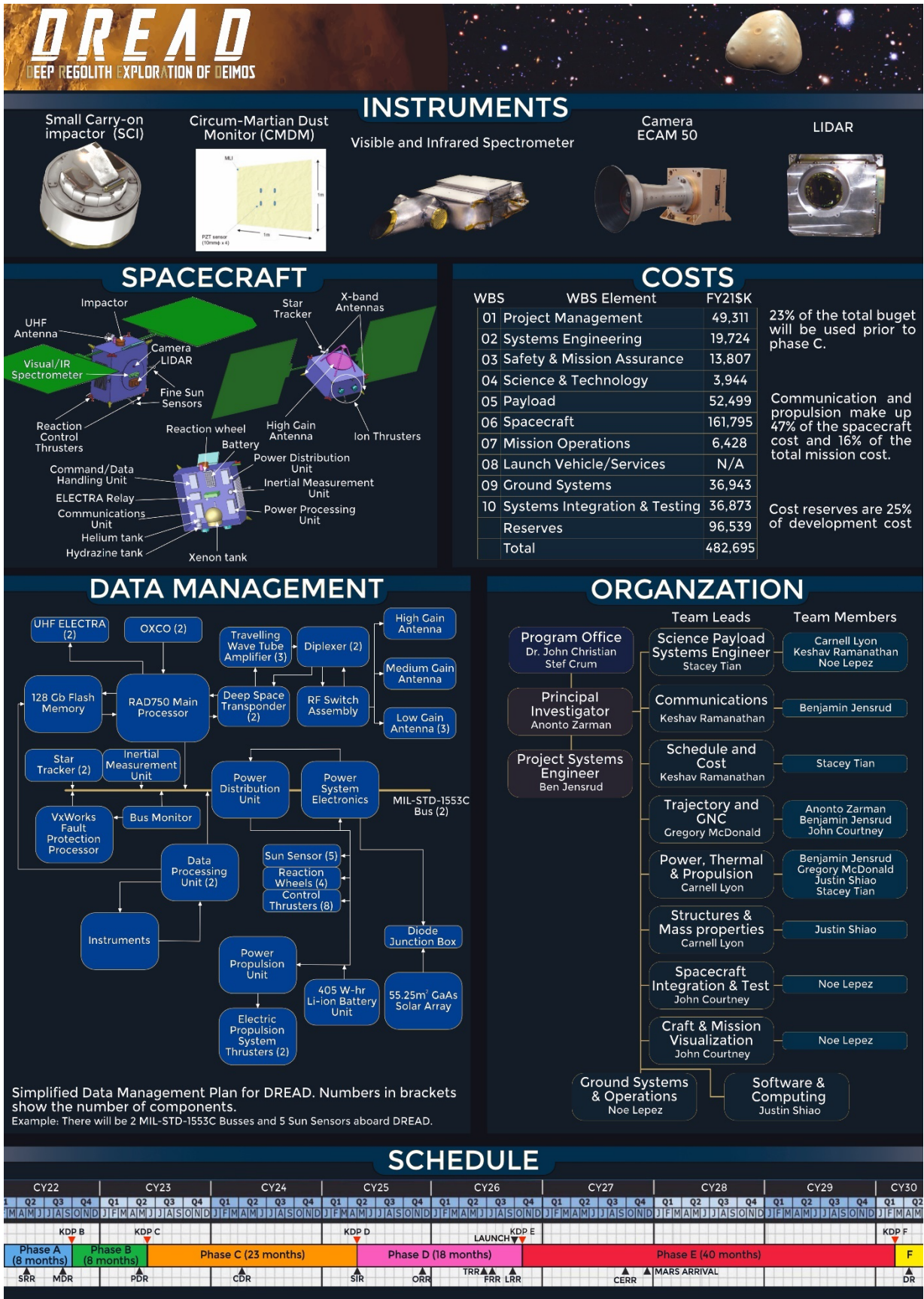


Table of Contents

Fact Sheet	1
Table of Contents	3
Science Investigation.....	4
Introduction.....	4
Deimos Background – Origins, Composition and Properties.....	4
Deimos Background – Potential for Crewed Missions.....	5
Mission Statement.....	6
Baseline and Threshold Mission.....	6
Science Traceability Matrix.....	7
Concept of Operations	10
Mission Implementation.....	11
Payload Instrumentation	11
Visible Light and Infrared Spectrometer.....	11
Camera.....	11
LIDAR System	11
Small Carry-on Impactor (SCI)	12
Circum-Martian Dust Monitor (CMDM)	12
Propulsion	13
Trajectory	14
ADCS	15
Power	16
Thermal Systems.....	18
Spacecraft Structure.....	19
Mass Budget.....	20
Software and Onboard Computing	22
Communications	23
Spacecraft and Mission Visualization.....	25
Data Management and Archiving	27
Integration and Test	27
Risk Analysis	27
Management	29
Cost and Schedule	31
Gantt Chart.....	31
Cost Tables.....	32
References	35

Science Investigation

Introduction

For decades, significant resources have been expended to characterize the properties, processes, and history of Mars. A vast variety of spacecraft have been developed to study Mars, including the Mars Reconnaissance Orbiter, InSight lander, and Curiosity and Perseverance rovers. Further missions are being developed to return samples and ultimately launch crewed Mars missions in the 2030s [1]. Despite the wealth of resources that have been devoted to studying Mars, comparatively little is known about its moons, Phobos and Deimos.

Images of Phobos and Deimos were first taken by the Mariner 9 spacecraft in 1971, followed by additional image data gathered by the Viking spacecraft a few years later. The Soviet Union planned the Phobos 2 spacecraft in 1988 but it ultimately failed to land on the moon. Additional observations of Phobos have been taken by the Mars Global Surveyor, Mars Reconnaissance Orbiter, and Mars Express Spacecraft. That said, comparatively little data has been collected regarding Deimos, owing to its higher orbital altitude [2]. One image of Deimos taken by the Mars Reconnaissance Orbiter is shown in Figure 1. Future missions to study Mars' moons include the Mars Moon eXplorer (MMX), currently organized by JAXA. The mission will be launched in the early 2020s and aims to return a sample from Phobos [4].

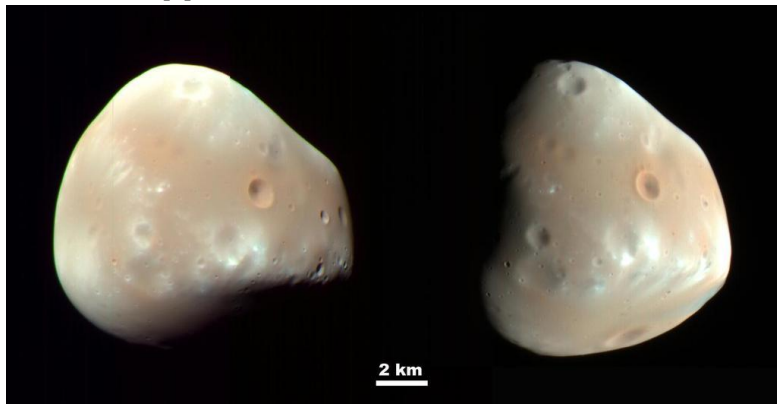


Figure 1. Note the relative lack of detail and low resolution of this image of Deimos taken by the Mars Reconnaissance Orbiter [3].

Though both of Mars' moons are promising locations for exploration, Deimos in particular is a fascinating platform for future missions. Whereas previous Mars-focused missions have successfully imaged Phobos, comparatively little data has been obtained for Deimos. Determining the origins of Deimos and characterizing the body's potential for human habitation will play a key role in understanding the formation of the Solar System and planning for crewed missions to the Martian surface.

Deimos Background – Origins, Composition and Properties

Phobos and Deimos are the only two natural satellites of terrestrial planets in the Solar System, other than Earth's Moon. As mentioned previously, little is known about Deimos' history. Three prevailing theories exist regarding the body's origins, the first being that it was a captured asteroid, the second being that it co-accreted with Mars, and the third being that it formed due to a collision between Mars and some small body. With a thorough investigation of the surface of Deimos and an analysis of its composition, the body's origins can be better understood [5]. Furthermore, determining Deimos' origin will provide key insights into how the Solar System developed and what processes encourage the formation of planets and other bodies in space.

The captured asteroid theory, suggested by William Hartmann, contends that Deimos was previously an asteroid and began orbiting Mars after entering its sphere of influence. The captured asteroid hypothesis is supported by Deimos' low density, low albedo, and spectral similarity to bodies in the outer asteroid belt [6]. The physics of the asteroid capture process, however, are difficult to explain dynamically, as the body must undergo sufficient energy loss in order to enter permanent orbit around Mars [7]. Furthermore, the surfaces of Phobos and Deimos are very similar, meaning that they may have had the same origin or were subjected to extensive space weathering [5].

The co-accretion theory, suggested by Joseph Burns, contends that Deimos emerged alongside Mars during its planetary formation process [8]. Under the co-accretion framework, Mars and Deimos are composed of similar materials, with Deimos reaching its small size due to successive impacts from planetesimals. A key advantage of the framework is that it lacks the dynamical challenges of the captured asteroid theory [5].

Most recently, the theory that Deimos formed due to an impact event has emerged. As explained by Robert Craddock, the impact-theory is supported by several key observations. Mars' high angular momentum suggests that a large body collided with the planet early in its history to generate its current spin rate, consistent with the presence of

several large craters on the Martian surface. Had a body impacted Mars with a sufficient velocity, a large amount of material would have been ejected into its orbit, forming an accretion disk and ultimately forming Deimos. The moon's orbital properties, which are difficult to explain using the captured asteroid theory, would have naturally resulted from the accretion process around Mars [9].

To distinguish between the different origin theories, the composition of Deimos needs to be better understood. The presence and relative concentrations of carbon, zinc, and magnesium will provide clues as to whether the body was captured from the outer or inner Solar System. Had Deimos co-accreted, the composition would be similar to bulk Mars, with the presence of magnesium and iron silicates. Finally, the asteroid impact theory would be indicated by high concentration of aluminum and calcium silicates but a lower concentration of iron silicates [5].

Investigating Deimos' history and composition is directly related to some of the critical goals mentioned in Small Bodies Assessment Group (SBAG) 2020 Goals and Objectives document [10]. This investigation falls under SBAG Goal 1, which asks to "investigate the Solar System's formation and evolution and advance our knowledge about the early Solar System conditions necessary for the origin of life through research and exploration uniquely enabled by small bodies." Gaining an understanding of the composition of Deimos relates to Objective 1.1, asking for "a study [of] elemental, isotopic, mineralogical, and molecular composition on [Deimos]". This understanding of the composition of Deimos also correlates to Objective 1.3, which emphasizes the "measure[ment] of volatiles (including, but not limited to, water, organics, other H, C, N, O and S bearing species and noble gases) in [Deimos]", which, as discussed, enables the determination of its origins.

Characterizing the physical properties of Deimos is also vital to a successful science mission and is mentioned in SBAG under Objective 14.1 as "understand the structure of the surfaces of small bodies, including roughness and surface compaction state, in various locations in the Solar System, and how chemical and physical properties are modified by the space environment." This is also specified in Objective 14.2, which states the need to "understand the overall physical properties of small bodies, including size, shape, mass, density, porosity, and spin rate." Finally, investigation into Deimos is highlighted specifically by Goal 1 Supplement D in SBAG, placing an emphasis on science questions such as "what are the origins of...Deimos", "what are the elemental and mineralogical compositions of...Deimos and how do[es it] vary between color units?", "what are the physical and surface properties of...Deimos?", and "how do Phobos and Deimos relate to other bodies in the Solar System?". Investigating the origins, the composition, and the physical properties of Deimos is crucial to advance scientific knowledge of Mars and the broader Solar System [10].

Deimos Background – Potential for Crewed Missions

Though much effort has been geared towards human exploration of Mars, Deimos itself is also a valuable location for crewed operations. Crewed missions to Mars' moons may serve as a stepping stone for future missions to the Martian surface. They may also enable further communication to Mars and serve as sources for in-situ resources. Between Mars' two moons, Deimos is the more promising location for crewed operations because it has an orbital radius of approximately 23,460 km, far greater than Phobos' orbital radius of 9,377 km, shown below in Figure 2. Because of its larger radius, Deimos is easier to land on, is sunlit more often, and has better communications access. Additionally, the delta-V for an Earth-to-Deimos mission is approximately 400 m/s less than that of an Earth-to-Phobos mission [11]. Despite Deimos' potential as a location for human exploration, significant research is needed before a crewed mission can be realized. In particular, Deimos' debris field, gravity and rotational environments need to be better understood.

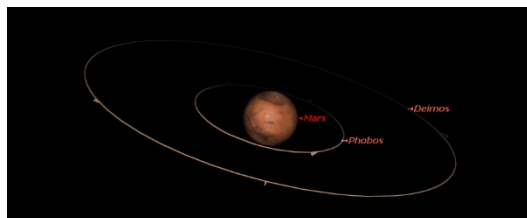


Figure 2. Deimos' large orbital radius reduces its time in Mars eclipse which improves accessibility [12].

Understanding Deimos' debris environment will be crucial for protecting astronauts from potential impacts. Analysis of Phobos indicate that Mars impact ejecta collide with the moon at velocities of approximately 2-3 km/s. Secondary impacts on Phobos then produce ejecta with velocities of approximately <800 m/s, meaning that over 95% of Phobos' ejecta remains in orbit about Mars. Because of Deimos' greater orbital radius, lower-velocity impacts would be expected, but it is crucial nonetheless to understand the ejecta environment about the body [7]. Models of Deimos suggest the presence of Martian dust rings about its

orbit, but no observational evidence has been found. Verification of surface dust models is needed through a combination of dust monitors and optical cameras [13].

The gravity and rotational environments of Deimos must be understood in order to develop instrumentation, deploy equipment, and map viable areas for human exploration. Small bodies, including Deimos, are known for their irregular shapes, high spin rates, and low mass, making human navigation difficult without a priori analysis. Furthermore, Deimos' microgravity environment will present health and operational challenges to astronauts. The lower gravity, however, will also improve the prospects for exploration as crater walls will have shallower slopes. This will make them easier to traverse and simpler to set up crewed base camps [7].

The importance of Deimos for human exploration is further reflected in the 2020 SBAG Goals and Objectives document [10]. In particular, SBAG Goal 3 highlights the need to "advance our knowledge of potential destinations for human exploration within the small body population and develop an understanding of the physical properties of these objects". Within the broader human exploration goal, Objective 3.2 specifies the need to characterize Deimos' environment for extended proximity operations and its surface physical characteristics. To accomplish this, the group explains that future missions must "obtain in-situ, high-resolution images of the specific target in question to determine rotation state and presence of co-orbitals/natural satellites... conduct topographic mapping for surface feature characterization... [and] perform detailed radio science mapping of the target's mass distribution and gravity field". SBAG also specifies that, "dust in the small body environment may act as both a hazard and a nuisance, especially given [its] known physical, chemical, cohesive, and electrostatic properties". As such, the science needs to characterize Deimos' gravity field and dust concentrations directly link to the broader SBAG objectives for human exploration.

Regarding Deimos in particular, SBAG Objective 3.4 emphasizes the need to "characterize [its] surface and near-surface composition and geotechnical properties". Sub-surface measurements in particular will prove crucial as the moons may serve as a source for in-space propellant. Indeed, document further stresses that "the presence or absence of useful propellant resources would substantially change the design, cost, and timeline of missions that involve sending astronauts to Mars" [10]. Deimos' importance as a base for crewed Mars exploration is a pressing science need and a key component of SBAG's goals for small body exploration.

Mission Statement

Project DREAD (Deep Regolith ExplorAtion of Deimos) will use an orbiter to investigate the formation of Deimos and to evaluate its viability for human exploration. Imaging techniques will be used to determine its composition on and below its surface. Sub-surface measurements will be taken through investigating the impact crater following impactor collision.

Baseline and Threshold Mission

DREAD's baseline mission is to use an orbiter to investigate the formation of Deimos and to evaluate its viability for human exploration by fully imaging the surface of the moon, performing radiometry, and sending an impactor to take sub-surface measurements. The baseline science mission duration will be two years with options to descope to a single year in the interest of reducing mission cost, risk, and spacecraft mass.

DREAD will provide a vast amount of evidence to further understanding of the composition, formation, and processes of Deimos. The data will also aid in understanding the formation of Mars and other bodies in the Solar System. Furthermore, Deimos's location within the Solar System is extremely advantageous for future crewed missions to Mars and beyond. DREAD will determine whether Deimos can serve as a viable hub for in-situ resource utilization, communications, and transport for future missions, enabling human exploration of the Solar System.

As part of the imaging process, DREAD will take surface images of Deimos with a ground sample distance of 2.5 m for a baseline mission. For the threshold mission, the ground sample distance can be increased to 5 m. By descoping to a lower resolution camera, DREAD will be able to save mass and cost, while still fulfilling its main purpose of imaging the entirety of the moon. In addition to the surface images, DREAD will also determine the topography of Deimos. Deimos has a unique appearance and detailed knowledge of its surface will contribute to understanding of what processes led to its current state.

DREAD will also determine the composition at the surface of Deimos and the distribution of these materials across the entire moon. As a baseline mission, spectroscopy will be performed with a spectral range of 380 nm to 2500 nm, with the option to descope to a narrower band of wavelengths, saving mission cost and reducing the spectrometer

complexity. Following impactor collision with Deimos, DREAD will also analyze the sub-surface composition of the moon by imaging the resulting crater.

A possible descope to the threshold mission involves removing the impactor. This descope will still allow for a full understanding of Deimos' surface composition, from which conclusions regarding its formation can be drawn. Surface measurements will also enable simplified analysis regarding the presence of resources relevant to human exploration. By removing the impactor portion of the mission, DREAD can save mass and cost while also alleviating the risks associated sending a projectile and creating debris. Furthermore, this descope can take place early on in the mission lifecycle, to reduce spacecraft mass and cost, as well as during mission operations, should the unstable orbital mechanics around Deimos result in an impactor maneuver that is too high risk.

In addition to the imaging, DREAD will also perform gravity and radio science to evaluate whether the gravitational field around Deimos allows for a safe human presence. Knowledge of the gravitational field will also allow the mass and therefore, density of Deimos to be determined, which contributes to the analysis of the formation hypotheses.

To further evaluate the viability of human exploration of Deimos, DREAD will measure the dust flux in the vicinity of the moon to determine if a safe human presence is possible. However, in the interests of cost and spacecraft mass, these measurements can be eliminated as a descope option without compromising the primary science goals of the mission.

Science Traceability Matrix

The DREAD Mission will collect science data to further Objectives 1.1, 1.3, 1.4, 3.2, 3.3, and 3.4 of the goals and objectives identified by the Small Bodies Assessment Group in 2020. Objectives under Goal 1 are related to understanding the formation and current composition of Deimos and those under Goal 3 are connected to human exploration efforts. The full Science Traceability Matrix for the DREAD Mission is presented below in Table 1.

In order to determine which of the formation hypotheses proposed by Craddock [9], Murchie [5], or some other theory is the most justifiable, DREAD will use a Visible Light and Infrared Spectrometer to determine the surface composition of Deimos. The spectrometer will have a spectral range from 380 nm to 2500 nm, aligning with observations presented by Takir [14], to investigate the presence of water, hydroxyls, organics, and carbonate minerals on Deimos and its distribution across the moon. The spectrometer will also be used to determine whether sufficient volatiles are present on Deimos to be used as in-situ resources for human exploration missions [7]. DREAD will also carry an impactor, which will create a crater on Deimos. Spectrometry will also be performed at this crater site to determine the sub-surface composition of the moon.

DREAD will also include a camera to fully image Deimos. These images will be used to estimate the volume of Deimos, to determine its topography, and to identify its rotation state. The volume measurements will help determine the density of Deimos to a greater accuracy, adding to evidence for the formation hypotheses. The topography of Deimos will allow for further understanding of which processes occurred on the moon that resulted in its unique appearance and properties. The processes that are currently suggested include weathering, creep, and gardening [15]. Finally, the viability for a safe human presence on Deimos can be evaluated using understanding of its rotation state.

The topography of Deimos will be determined to a higher fidelity through mapping its surface using a LIDAR system. From this map, the surface roughness of the moon can also be found. Data from the LIDAR system, in addition to that from the spectrometer and camera, will be used to determine the impactor site.

To further evaluate the feasibility of a safe human presence on Deimos, DREAD will fly a dust monitor, which will determine the size and flux of particles around the moon. Liu et al. has suggested that particles near Deimos are within 5 to 20 μm [16].

Finally, radiometry will be performed using the antennae of the communications system to measure doppler shifts. Measurement of these frequency shifts will allow the gravitational field around Deimos to be determined, which will be used to evaluate its safety for human presence, as well as the mass of Deimos, which will be used in density calculations.

Table 1. As can be seen from the STM, with 5 science instruments, DREAD will be able to achieve a broad range of science objectives, which are derived directly from SBAG goals and objectives.

Science Goals	Science Objectives	Science Measurements Requirements		Instrument requirements	Projected Performance	Mission Requirements
		Physical Parameters	Observables			
Understand the processes that led to the formation and current composition of Deimos, as highlighted in SBAG 2020 Goal 1, Objective 1.1, Objective 1.3, and Objective 1.4	Determine whether Deimos was reaccreted from Mars ejecta [9], captured as an object from the asteroid belt [5] or developed in some other way based on its physical characteristics	Composition	Wavelengths of NIR absorption from	Spectral range	780 nm - 2500 nm	DREAD shall detect NIR absorptions of wavelengths between 780 nm and 2500 nm with a resolving power of at least 150.
			Wavelengths of visible light emission	Spectral resolution	R ≈ 150	
		Density	Radio wave frequency shift for mass	Frequency range	380 nm - 750 nm	DREAD shall detect visible light emissions of wavelengths between 380 nm and 750 nm with a resolving power of at least 125.
			Images of Deimos for volume	Shift	R ≥ 125	
	Determine whether volatiles such as water/hydroxyl, organics, and carbonate minerals, are present in Deimos [14].	Mass	Radio wave frequency shift for mass	Angular resolution	X-band frequencies	DREAD shall measure doppler shifts to an accuracy of at least 0.0596 mm/s using x-band frequencies.
			Frequency range	σ ≤ 0.0596 mm/s	X-band frequencies	
		Composition	Wavelengths of NIR absorption	σ ≤ 0.0596 mm/s	σ ≤ 0.0596 mm/s	DREAD shall image Deimos with an angular resolution of at least 0.28 radians/pixel.
			Wavelengths of visible light emission	Spectral resolution	R ≈ 150	
		Detect volatiles	Wavelengths of NIR absorption	380 nm - 750 nm	380 nm - 750 nm	DREAD shall detect NIR absorptions of wavelengths between 780 nm and 2500 nm with a resolving power of at least 150.
			Spectral resolution	R ≥ 125	R ≥ 125	DREAD shall detect visible light emissions of wavelengths between 380 nm and 750 nm with a resolving power of at least 125.
Understand whether the surface and environment of Deimos could serve as safe locations for human-oriented activities, as highlighted in SBAG 2020 Goal 3, Objective 3.2 and Objective 3.3	Determine whether the properties of Deimos's surface resulted from weathering, creep, gardening, or some other process [15].	Roughness	Morphological features	Spectral range	780 nm - 3600 nm	DREAD shall detect NIR absorption lines of wavelengths between 780 nm and 3600 nm with a resolving power of at least 200.
			Vertical resolution	780 nm - 3600 nm	R ≈ 200	
			Sampling rate	R ≈ 200	R ≈ 200	DREAD shall map the topography of Deimos with a vertical resolution of at least 0.5 m and a sample rate of at least 1 Hz
			Morphological features	Vertical resolution	>= 0.5 m	DREAD shall map the topography of Deimos with a vertical resolution of at least 0.5 m and a sample rate of at least 1 Hz
			Sampling rate	>= 0.5 m	>= 0.5 m	DREAD shall image Deimos with an angular resolution of at least 0.28 radians/pixel.
	Determine if the rotation state of Deimos allows for a safe human presence on the moon [7].	Topography	Morphological features	Angular Resolution	>= 0.5 m	DREAD's cameras shall have a field of view of at least 80°.
			Surface images	Angular Resolution	>= 0.5 m	
			Surface images	Sampling rate	>= 1 Hz	DREAD's cameras shall have a frame rate of at least 1 image/second.
			Surface images	Sampling rate	>= 1 Hz	
			Surface images	Angular Resolution	<= 0.28 radians/pixel	
Understand how humans could utilize Deimos' resources to further human exploration efforts, as highlighted in SBAG 2020 Goal 3, Objective 3.4	Determine if the gravitational field of Deimos allows for a safe human presence on the moon [7].	Rotation rate	Surface images	Field of View	<= 0.28 radians/pixel	DREAD shall image Deimos with an angular resolution of at least 0.28 radians/pixel.
			Surface images	Frame rate	> 80°	DREAD's cameras shall have a field of view of at least 80°.
			Surface images	Frame rate	1 image/second	DREAD's cameras shall have a frame rate of at least 1 image/second.
			Surface images	Angular Resolution	<= 0.28 radians/pixel	DREAD shall image Deimos with an angular resolution of at least 0.28 radians/pixel.
			Surface images	Field of View	> 80°	DREAD's cameras shall have a field of view of at least 80°.
	Determine whether the particulate torus around Deimos will be hazardous for human exploration [7].	Gravitational field	Doppler shift of radio waves	Frequency range	X-band frequencies	DREAD shall measure doppler shifts to an accuracy of at least 0.0596 mm/s using x-band frequencies.
			Doppler shift of radio waves	Shift accuracy	σ ≤ 0.0596 mm/s	
			Wavelengths of NIR absorption	Spectral range	780 nm - 2500 nm	DREAD shall detect NIR absorptions of wavelengths between 780 nm and 2500 nm with a resolving power of at least 150.
			Wavelengths of visible light emission from	Spectral resolution	R ≈ 150	
			Wavelengths of visible light emission from	Spectral range	380 nm - 750 nm	DREAD shall detect visible light emissions of wavelengths between 380 nm and 750 nm with a resolving power of at least 125.
Understand how humans could utilize Deimos' resources to further human exploration efforts, as highlighted in SBAG 2020 Goal 3, Objective 3.4	Determine whether there are sufficient relevant volatiles for Deimos to serve as an in-situ resource for human exploration missions, specifically to those to Mars [7].	Dust particle concentration	Dust particle concentration	Size of particles detected	Detect particles between 5-20 μm	DREAD shall detect dust particles of size between 5 to 20 micrometers
			Dust particle concentration	Dust Flux	Detect particles between 5-20 μm	
			Dust particle concentration	Size of particles detected	Detect particles between 5-20 μm	

Concept of Operations

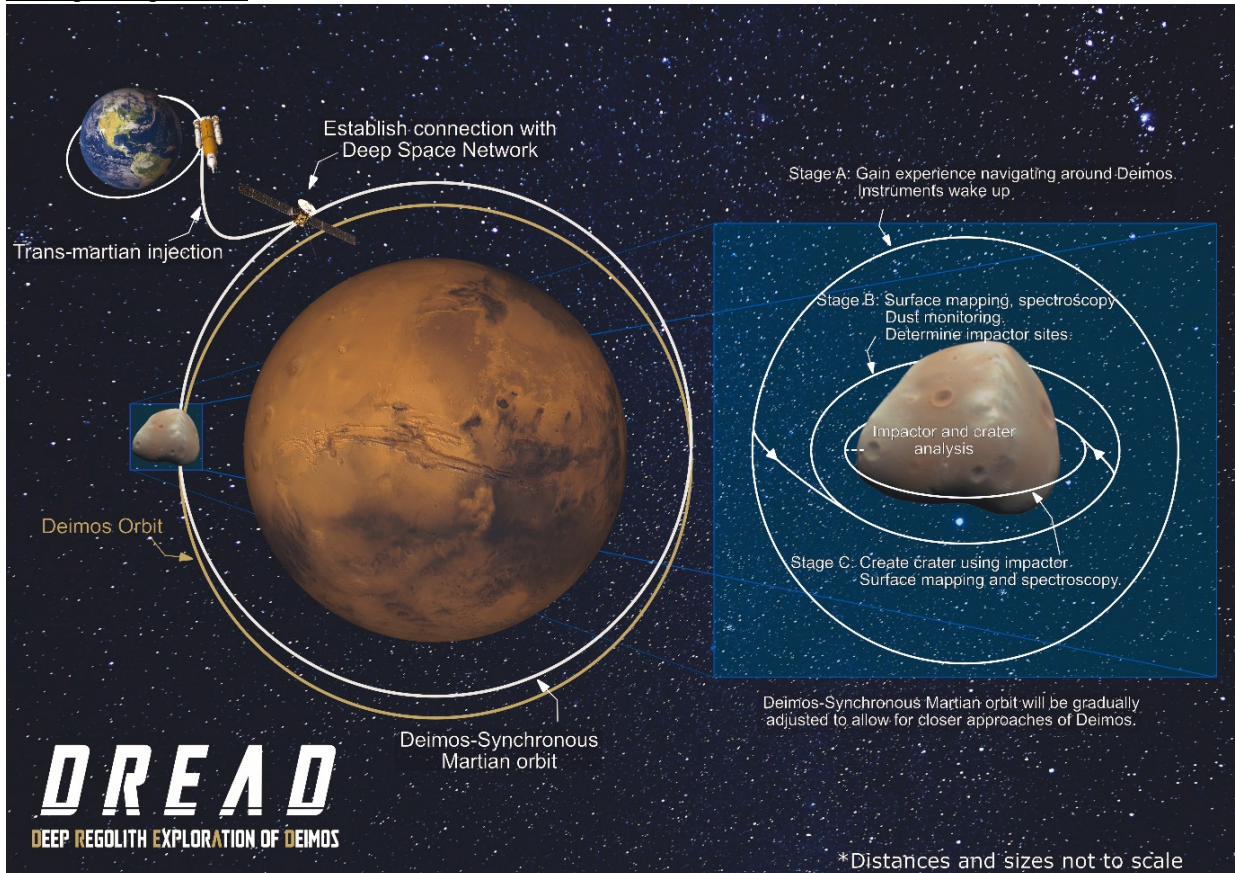


Figure 3. DREAD's primary orbit is tailored to limit stationkeeping required during a majority of its life cycle.

As shown above, in Figure 3, the DREAD mission will be split into three stages, A, B, C. Firstly, after reaching Martian orbit through a trans-Martian injection, DREAD will perform maneuvers to attain a Deimos-Synchronous orbit. This orbit enables the satellite to stay close to Deimos while still orbiting Mars, lowering the delta-V stationkeeping requirements. Throughout the initial one-to-two-month Stage A period, the instruments will wake up, and tests will be performed to ensure that they are properly functioning. Additional maneuvers and propulsion tests will be completed to gain experience navigating around Deimos.

Stage B begins once instruments are operating nominally. Over a one-year period, DREAD will map Deimos' surface, perform spectroscopy measurements of the surface, and monitor for dust particles to satisfy its science objectives. The spacecraft will use its propulsion systems to fine-tune its orbit and get closer to the Martian moon as needed. As the science phase ramps up, teams on the ground will analyze DREAD's data and search for suitable sites for impact cratering. A suitable site could appear to have unique characteristics from the spectroscopy data, such as having a larger (or lower) concentration of specific elements, lacking craters, or appearing to be softer, which could allow the impactor to create a deeper crater.

Finally, once DREAD's primary science objectives are complete and an impactor site has been chosen, the spacecraft will approach Deimos to drop the impactor. As the spacecraft needs to perform an escape maneuver to avoid being hit by impactor debris, the impactor will explode when its internal timer (set before separation) reaches zero. Once the countdown completes, the impactor will send a 2.5kg copper bullet into Deimos at a speed of 2km/s, creating a crater on the moon. DREAD will analyze the crater one month later to ensure it does not get damaged by dust or rocks thrown up by the impact. Once its science objectives are fulfilled, the spacecraft will enter a heliocentric graveyard orbit and complete operations.

Mission Implementation

Payload Instrumentation

Visible Light and Infrared Spectrometer

The Visible Light and Infrared Spectrometer that will be flown on DREAD will have a total mass of 17.8 kg and a power usage of 8.8 W. It will use the Teledyne H1RG, which is a hybrid CMOS detector made of HgCdTe. Using a pre-existing detector reduces costs and risks associated with developing a new spectrometer detector. The detector will have a pixel pitch of 18 microns and while the H1RG detector has a resolution of 1024 by 1024 pixels, only the center 512 by 512 pixels will be used [17]. The system will have a FOV of 2 milliradians, corresponding to a focal length of 4.6 m. This large focal length will be achieved using a series of curved mirrors. Therefore, at an altitude of 10 km, which is the minimum possible with the electric propulsion system, each sample will correspond to a ground resolution of 40 m by 40 m.

The sensor's incoming waves will be dispersed using a linear variable filter ranging from 380 nm to 2500 nm. The use of a filter as a dispersive element instead of a diffraction grating or prism will reduce the complexity of the system as well as its mass.

To fully image Deimos's surface, a total of 302,000 samples must be taken, corresponding to 79.17 GB of data per period and a pixel rate of 2,510 pixels per second, which is significantly below the maximum of 10Mpixels per second [18].

Following impactor collision with Deimos and the settling of the dust cloud, DREAD will take spectrometer measurements of the resulting crater from an altitude of 500m. A total of 2,412 samples will be taken during the remaining second year of the science mission, resulting in 632 MB of data.

This spectrometer is similar to the VIRTIS instrument flown on the Rosetta mission [19] and the OVIRS instrument from OSIRIS-REx [17].

Camera

The camera that will be used on the DREAD mission will have a mass of 12.25 kg and a power usage of 2.5 W. It will be a staring system using a CMOS detector that is built around the Malin Space Science Systems ECAM-C50 system. Using the ECAM-C50 system reduces overhead costs, increases reliability as it has already been flown in space, and reduces developmental risks. It will have a pixel pitch of 2.2 microns and a focal length of 4.4 mm, which results in an IFOV of 0.25 milliradians per pixel. The detector resolution will be 3400 by 3400, which will fulfil the requirement of a FOV of 80° by 80°. Since the MSSS ECAM-C50 has a data rate of 20 MPixels per second [20], DREAD's camera system will have a maximum frame rate of 1.74 images per second. However, at an altitude of around 10 km and based on the FOV, only 8 images of Deimos will be required to fully image the moon. This image rate will result in 92.48 MB of data. Furthermore, at this altitude, the camera will have a ground sample distance of 5 m.

Similar instruments that have already been flown on spacecraft include OSIRIS-REx's TAGCAMS system [21], Hayabusa's AMICA camera [22], and New Horizon's LORRI [23].

LIDAR System

DREAD's LIDAR system will have a total mass of 21.4 kg and require a maximum of 59 W of power. It will have a Silicon Avalanche Photodiode detector and will use a line scanning pattern in the direction perpendicular to the orbit of the spacecraft to increase coverage on Deimos. The system will operate at a maximum frequency of 100 Hz and output 14-bit values [24]. Each sample will have a circular footprint with a 1.4m diameter. Therefore, approximately 313,795,819 scans will be needed to fully image Deimos, resulting in 549.14 MB of data. To perform all these scans within the first year of the science orbits will result in a scanning frequency of less than 100 Hz.

This LIDAR system is comparable to MESSENGER's MLA [25], OSIRIS-REx OLA [24], and Hayabusa2's LIDAR system [26].

Small Carry-on Impactor (SCI)

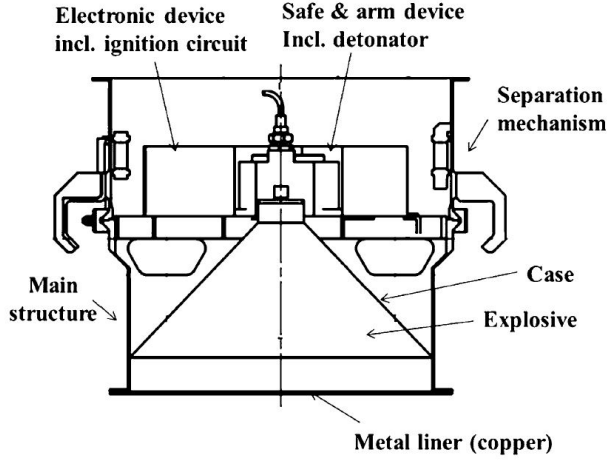


Figure 4. Outline of the Small Carry-on Impactor [27].

as shown in Figure 4. The electric section houses batteries, a sequencer, an ignition circuit, and solar panels outside. These solar panels are used as light detectors, which will begin the countdown once the SCI separates. Solar panels were used instead of a mechanical switch, as the switch could accidentally arm the SCI during turbulent phases of DREAD's path to Mars, which would result in the spacecraft's destruction.

The impactor will be used at the end of DREAD's science phase due to its associated dangers. Indeed, once an impactor site has been decided, the craft will descend and separate from the impactor. The SCI will approach the asteroid at a speed of 20 cm/s and with a spin rate of 75deg/s [28]. Once the SCI separates from the spacecraft, a timer set before separation will start to allow time for the mother spacecraft to move out of the impactor's line of sight. As such, DREAD will not be able to see the impactor explode or the crater being made. However, as the impactor will launch small metal fragments at high speeds in all directions, the satellite should not observe the impactor explosion due to the high risk it entails. Once the detonator ignites, the copper liner is blasted with such force it deforms into the shape of a bullet due to cold forging. The impact of the bullet flying at 2km/s is expected to create a crater of 2.5m to 6m in diameter.

Circum-Martian Dust Monitor (CMDM)

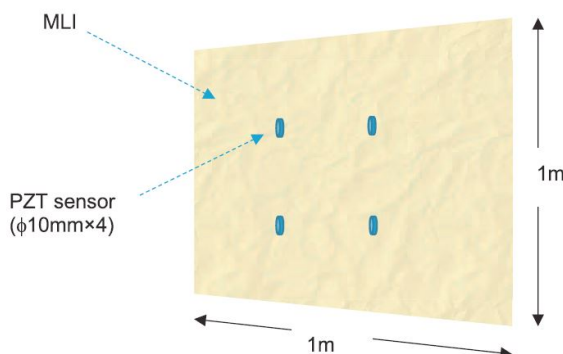


Figure 5. Concept image of the CMDM [29].

Mining under small gravity is difficult. Using a charge to blast the regolith away is another possibility; however, the pollution with chemical compounds will be an issue for soil analysis. As such, DREAD will use the Small Carry-on Impactor (SCI) to determine the weathering processes occurring on Deimos. Indeed, the SCI will create a crater on Deimos, which will allow DREAD to analyze how surface material changed due to weathering. In addition, these sub-surface measurements may provide a better understanding of Deimos' past and origins.

First used on JAXA's Hayabusa2 mission, the SCI is a lightweight but extremely powerful device capable of accelerating projectiles to speeds of 2km/s. It is made up of two parts, the explosive and the electric part. The explosive part comprises a 2.5kg copper liner case, behind which is a case filled with 4.5kg of cyclotetramethylene tetranitramine (HMX) [27], a powerful explosive,

[27]

The Circum-Martian Dust Monitor (CMDM) is an instrument currently being developed for JAXA's Martian Moons Explorer (MMX) mission, which is set to launch in 2024. The CMDM will be made up of a square 1m by 1m polyimide film with multiple piezoelectric (PZT) sensors. Once in operation, the instrument will detect dust particles by identifying the stress waves caused by the impact of small particles on the film. These will then be transformed into electronic signals by the piezoelectric sensors. Having at least 3 PZT sensors allows the sensor to determine the position of the wave source by calculating the difference between the arrival time of the signal. The sensor can use this information to distinguish whether it is a dust signal or noise from other sources [29].

Propulsion

DREAD will have various mission stages and burns that require significant delta-V allocation. Since stationkeeping around Deimos will continuously draw from the delta-V budget, liquid chemical and electric propulsion options were traded for the main propulsion system to maximize delta-V while minimizing propellant mass. In this case, the mass benefits of using Solar Electric Propulsion (SEP) outweigh the benefit of increased thrust and reduced cost that a liquid chemical system would grant.

The main propulsion system for DREAD is NASA's Evolutionary Xenon Thruster - Commercial (NEXT-C), which is a gridded ion electrostatic thruster designed for use with xenon as its propellant. It has a maximum specific impulse of over 4200s and is designed to operate at an input power of anywhere between 0.6 and 7.4 kW and a thrust range of 25 to 235 mN [30]. For redundancy and resilience against degradation, DREAD will employ two separate NEXT-C thrusters, but only operate one at a time. Each thruster is qualified to use the entire propellant flowthrough required, so to prevent loss of mission in the event one fails the two thrusters will be swapped between during any maneuvers to evenly degrade the protective coatings of the cathodes and maximize the lifetime of a surviving thruster. These main thrusters on DREAD will operate under different conditions for each mission segment since its closer proximity to the Sun during the trans-Mars insertion burn will provide more power for the thrusters. For the duration of its stay at Mars, the thrusters are expected to receive approximately 5.5kW and therefore be capable of approximately 170 mN of thrust. The xenon does not need to be fed in at high pressure and therefore does not need a separate pressurization system. The spacecraft will carry 525kg of xenon, corresponding to a total delta-V capability of 18.2 km/s.

The Attitude Control System (ACS) on DREAD was heavily based on NASA's 2009 Lunar Reconnaissance Orbiter [31]. The ACS utilizes 8 Aerojet MR-130D thrusters with 25 kg of hydrazine monopropellant and helium as the pressurant.

Shown in Figure 6 are the ACS and SEP propulsion systems that DREAD employs.

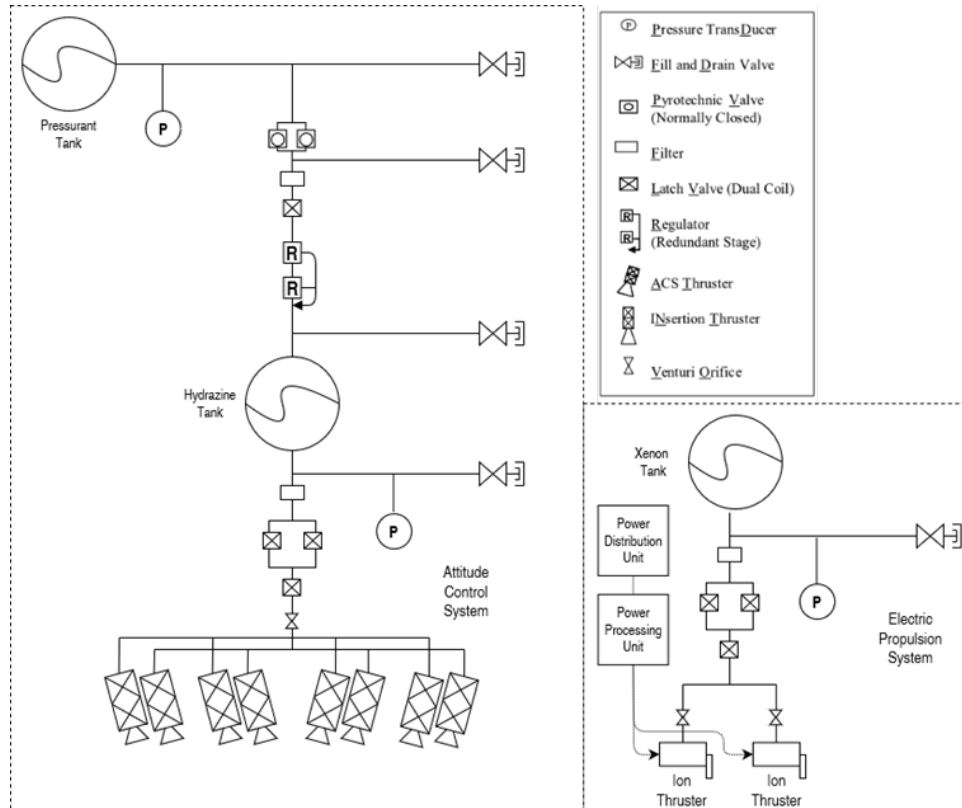


Figure 6. Main and Secondary propulsion system schematics. The use of the electric propulsion system allows for significant reduction in system complexity, and the attitude control system uses heritage design to minimize new development effort required.

Trajectory

The trajectory of DREAD consists of the initial transfer to Deimos, three science stages, and decommissioning. Due to having only 0.17N of thrust, the thrusters must operate for long periods of time and therefore cannot be assumed to be instantaneous impulsive burns. To simulate these long duration burns, NASA GRC's GMAT tool [32] was utilized.

DREAD will launch on the 17th of October 2026 on an escape trajectory with approximately $8 \text{ km}^2/\text{s}^2$. This will place it into an orbit close to Mars but with an apoapsis slightly lower than Mars' apoapsis. DREAD will coast until the 28th of May 2027 when it will activate its ion thrusters to begin accelerating. As it gets closer to Mars, it will gradually speed up to catch up with Mars's orbital velocity while simultaneously shifting its apoapsis forward, causing the orbit to have the same velocity as Mars when it eventually reaches the edge of its SOI on the 19th of December 2027. This burn is estimated to consume 2.48km/s of delta-V. The transfer phase is shown in Figure 7.

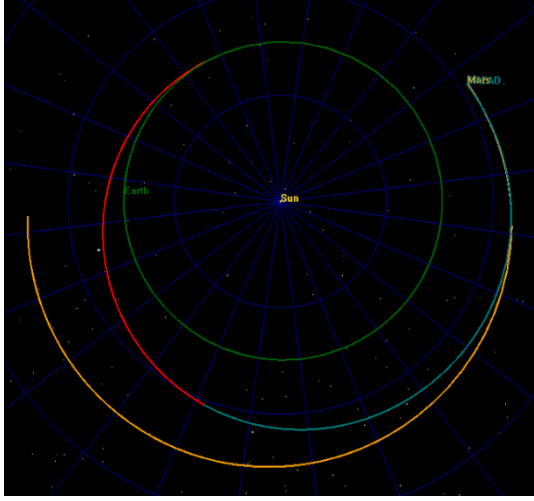


Figure 7. Earth-Mars Transfer Orbit bringing DREAD to Mars. Red is coasting, teal is thrusting.

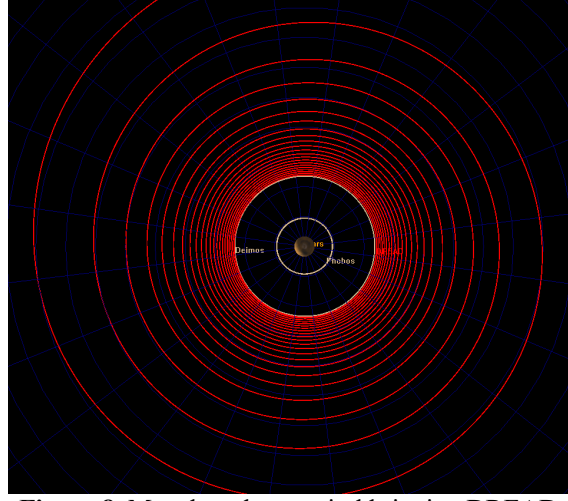


Figure 8. Mars low thrust spiral bringing DREAD from the edge of Mars SOI down to Deimos.

Once DREAD reaches the edge of Mars's SOI, it will still need to put itself in a lower circular orbit to reach Deimos. To achieve this, it will perform a low thrust spiral down from the edge of the SOI to Deimos's orbit, where the thruster will continuously run retrograde to gradually lower the orbit. This will last until the 26th of February 2028. The initial entry into Mars SOI will be targeted to achieve the correct inclination and ascending node right ascension such that it will be placed into Deimos's orbital plane without needing additional maneuvering. This also helps avoid entering Mars's shadow, although if any eclipse periods occur, they will be incredibly short (only a few minutes at worst) and the thrusters can safely be deactivated while they do not have solar power to simply continue with the burn on the other side. During the spiral, once the orbit is low enough that Deimos is visible in the instruments, Stage A science collection will begin to gather rough environmental and gravitational data from Deimos to begin navigation. This burn is estimated to consume 0.70km/s of delta-V. This phase is shown above in Figure 8.

Since Deimos has such low gravity compared to Mars's gravity gradient at its orbit, there are no normal Keplerian orbits possible around Deimos [33]. Therefore, when DREAD has reached Deimos, it will enter a Deimos-synchronous Mars orbit where the inclination, eccentricity, RAAN, and argument of periaxis about Mars are slightly varied to give a polar orbit-equivalent in Deimos' body fixed frame. To properly frame the instruments, DREAD will be in a close to circular orbit 10km above the largest dimension of Deimos (15km). The instruments will cover an area of approximately 1.4° of Deimos's surface at its equator, so DREAD will adjust its orbit by that amount each orbit (not including downlinking orbits) to gradually cover the entire surface. This means DREAD will cover the full surface of Deimos within one year of science operations. The stationkeeping for this orbit is estimated to consume 4.78km/s of delta-V. An example orbit from this phase is shown in Figure 9.



Figure 9. Deimos-synchronous Mars orbit shown in the Deimos body-fixed frame, allowing complete surface coverage of Deimos.

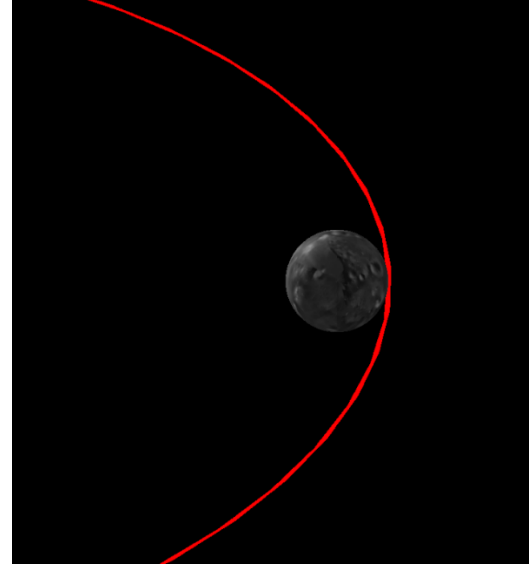


Figure 10. Low passes over impact site giving high resolution of impact crater.

Once a complete surface map is obtained, a location will be selected for the impactor. The orbit will then be lowered, and a short burst from the hydrazine thrusters will stop DREAD above the surface. The impactor will then be released, and the hydrazine thrusters will once again burn to put DREAD back into orbit. These two burns will utilize approximately 10 m/s of delta-V from the hydrazine thrusters. The impactor will be timed for DREAD to orbit around to the other side of Deimos to avoid any of the debris that will be generated from the impactor. After waiting for the debris to settle, DREAD will then place itself into its Stage C orbit, consisting of a close to elliptical orbit with its closest approach directly above the impactor site. This will allow for higher resolution of the impactor site while not requiring as much stationkeeping fuel as a purely lower orbit. The stationkeeping for this orbit is conservatively estimated to be the same as the Stage B 10km orbit, 4.78km/s of delta-V. A close-up of this orbit is shown in Figure 10.

Once the science portion of DREAD's mission is finished, DREAD will put itself into a heliocentric graveyard orbit to avoid contamination of Mars or its moons. This will be the reverse of the low thrust spiral in and will require a similar amount of delta-V, approximately 0.70km/s.

A total accounting of all delta-V accounting is presented in Table 2. Since the gravitational environment of Deimos is highly speculative, there is a high likelihood more is required, especially during the stationkeeping phases. Therefore, significantly more is included, as shown in the propulsion section. In addition, since the gravity and distances are so small in the vicinity of Deimos the individual maneuvers to adjust between science orbits require only single digit delta-V expenditures to accomplish and therefore are not individually accounted for.

Table 2. Trajectory plan demonstrating total delta-V requirements.

Segment	Timeline	delta-V Required (km/s)
Earth-Mars transfer	17 Oct 2026 – 19 Dec 2027	2.477
Mars SOI to Deimos spiral	19 Dec 2027 – 16 Feb 2028	0.696
Stage B orbit	16 Feb 2028 – 16 Feb 2029	4.778
Stage C orbit	16 Feb 2029 – 16 Feb 2030	4.778
Heliocentric graveyard orbit	16 Feb 2030 – 16 Apr 2030	0.696
Miscellaneous maneuvering	-	1
Total	17 Oct 2026-16 Apr 2030	14.425

ADCS

Previous missions that have explored the Mars system have either used exclusively reaction control thrusters (i.e., Mars Global Surveyor) or have used a combination of reaction wheels for pointing with reaction control wheels for

momentum dumping. The DREAD mission will be implementing the latter strategy to reduce the amount of propellant needed to operate over its three and a half-year life cycle by using four reaction wheels. Since the relative orbital period around Deimos is 30 hours long, the ADC System onboard DREAD will only need to make one rotation every 30 hours in addition to resisting solar pressure and the gravity gradient when near Deimos while conducting its science mission. This has the added benefit of requiring a smaller amount of hydrazine propellant to dump the momentum built up in the reaction wheels rather than full attitude control throughout the mission.

DREAD will be implementing a suite of star trackers and redundant fine sun sensors in addition to an inertial measurement unit to provide 1.5 arc second attitude precision [34]. The five sun sensors onboard the spacecraft bus are distributed on the five sides of the rectangular spacecraft bus, excluding the top face, which is occupied by the high gain antenna. Each CT-2020 star tracker is capable of maintaining its 1.5 arcsecond accuracy under slew rates below 8 degrees per second [34]. As mentioned, during nominal operations, the spacecraft will make one rotation every 30 hours which puts DREAD's slew rate well below this maximum.

A preliminary ADCS sizing analysis was performed to verify the amount of torque needed to maintain nadir pointing during science operations in addition to determining the amount of hydrazine propellant needed for momentum dumping operations during DREAD's mission life cycle. The spacecraft must be able to rotate at a slew rate of 12 arc seconds every second during science operations. Using the following expression for required torque, T_{req} , given rotation angle, θ , moment of inertia, I , time, t , and safety factor, F , of 10:

$$T_{req} = 4F\theta \frac{I}{t^2}$$

results in a required torque of $3.476 \times 10^{-5} Nm$ which is well below the maximum torque of the selected Honeywell HC7 reaction wheel. The required torque was then multiplied by the three and a half-year mission lifecycle to provide a conservative number for the total momentum dumping that the reaction control thrusters would need to provide during the mission life cycle. Based off the specific impulse and thrust ranges of the Aerojet Rocketdyne MR-103D thrusters [35], it was found that the total amount of propellant needed for momentum dumping was 842 grams. Due to the small amount of propellant needed for momentum dumping, additional propellant was allocated for when shorter duration maneuvers, such as the release of the impactor and pointing maneuvers needed for communications. It should be noted that this preliminary study does not consider the attitude changes needed for the thrust spiral maneuver to reach our Deimos synchronous orbit or the circularization of the Martian transfer trajectory since the NEXT-C ion engines will be utilizing their own gimbals to perform these maneuvers. In addition to this, the science instruments that were selected will be outfitted with their own gimbals to allow for slew rates independent of the main spacecraft bus. Since these torques are limited to small portions of the spacecraft, it is assumed that the required momentum dumping is negligible.

As mentioned before, the two Ball Aerospace CT-2020 star trackers provide a pointing accuracy of 1.5 arcseconds. In the event that both star trackers fail, the spacecraft is outfitted with five sun sensors to serve as redundant aids to the Honeywell MIMU Inertial Measurement Unit. Fine sensors were selected over passive coarse sun sensors to provide the highest degree of precision necessary to maintain the spacecraft's low slew rate. It should be noted that the precision of the Bradford Aerospace fine sensors onboard DREAD will be less than that of the CT-2020 Star Trackers [36]. Thus, the slew rate in the event of star tracker failure may not meet the baseline science mission but will still be sufficient for the threshold communications and maneuver pointing requirements. This is the motivation for introducing a redundant star tracker and reducing the risk of losing pointing accuracy.

Power

The power, shown below in Table 4, highlights anticipated power usage for five various spacecraft modes. The three nominal operations modes correspond to Stage B and C science orbits around Deimos. In these modes, all science instruments are on. Downlink and propulsion systems are toggled on and off so each possible configuration during data collection can be analyzed and planned for. The transfer mode will be used on DREAD's trajectory to Mars orbit and during the spacecraft's spiral toward Deimos's orbital radius. In this mode, the propulsion and ADCS systems are at full power, but no science instruments are recording data and the communications system is operating at reduced power. Safe mode is DREAD's minimum power mode that is only intended for use during emergency scenarios. Both the structure and thermal subsystems use only passive control, so they do not require power in any configuration. A 25% margin is used for all power modes, which is on the lower side for pre-Phase A missions, but was a necessary

choice given the large power requirements for the electric propulsion system. As discussed, a larger margin would produce too many difficulties for solar panel sizing and cost.

DREAD has selected Spectrolab ultra triple junction gallium arsenide solar cells for the solar array. These have a very high efficiency of 28.3% and are TRL9 – over 675 kW of these arrays have been launched into orbit [37]. With this efficiency factor and the other parameters shown in Table 3, the required solar panel size of 55.25 m² was calculated. The eclipse time of 12.89% assumes a 10 km altitude in Stage B and approximates Deimos as a sphere with radius 6.5 km. Additionally, the relative motion of Deimos was not considered because for a polar orbit this should be nearly perpendicular to the spacecraft’s motion. The solar panels were sized to handle the maximum power mode (nominal + propulsion + downlink) for the daylight period, plus charge a secondary battery system to be used during darkness. Due to the large power requirements of DREAD, the battery system was only equipped to handle nominal operations without propulsion. This means the ion thrusters can only operate during periods of daylight; while this constraint is somewhat limiting, eclipse periods are a maximum of about five hours and forgoing stationkeeping maneuvers during this time should not be problematic. While a 55 m² array is large, other planetary missions, including JUNO, have used solar panels of this size with success. DREAD has laid out a plan to fold the two solar panels into the launch vehicle fairing.

The selected battery cells are LG Chem INR18650, a rechargeable lithium-ion battery with specific energy of 266 W·hr/kg. This value is consistent with many state-of-the-art battery cells, and although high energy density cells do experience higher performance degradation, this should not be an issue within DREAD’s 3.5-year life cycle [38]. The required power of 848.50 W, darkness time of 3.91 hours (calculated from orbital eclipse proportion), and depth of discharge of 0.8 gives a required battery capacity of approximately 4 kW. However, a 50% margin is allocated because the eclipse periods during the lower altitude orbit in Stage C will be slightly longer. The total required battery capacity is 6278.34 W, corresponding to a battery mass of about 24 kg. The mass of the PMAD system is produced by scaling up the AAC Clyde Space Starbuck Mini (peak power output 1200 W) to meet the power requirements of DREAD.

Table 3. The following values were used to calculate solar array size for the selected GaAs cells.

Property	Value
Tau (mission duration in years)	3.5
Degradation per year	2.75%
BOL Power (W)	7725.4
EOL Power (W)	8517.4
Pointing efficiency	0.95
Cell efficiency	28.3%
Solar constant (W/m ²)	1353
Mars distance (AU)	1.52
% of orbit in eclipse	12.89%

Table 4. The power budget displays design limit values for each of the 5 power modes, broken down to Level 3.

	Nominal+P+D	Nominal+D	Nominal	Transfer	Safe
1.0 Payload					
1.1 Science Instruments					
1.1.1 Visible Light & IR Spectrometer	8.80	8.80	8.80	0.00	0.00
1.1.2 LIDAR	59.00	59.00	59.00	0.00	0.00
1.1.3 Dust Monitor	3.00	3.00	3.00	0.00	0.00
1.2 Cameras					
1.2.1 Detector	0.30	0.30	0.30	0.00	0.00
1.2.2 Optics and Electronics	2.20	2.20	2.20	0.00	0.00
1.3 Impactor					
1.3.1 Copper Lining	0.00	0.00	0.00	0.00	0.00
1.3.2 Propellant	0.00	0.00	0.00	0.00	0.00
1.3.3 Electronics and Structure	0.10	0.10	0.10	0.00	0.00
2.0 Spacecraft Bus (dry)					
2.1 Propulsion					

2.1.1 Thrusters	4501.00	0.00	0.00	4501.00	0.00
2.1.2 Gimbal	0.39	0.00	0.00	0.39	0.00
2.1.3 Power Processing Unit	500.00	0.00	0.00	500.00	0.00
2.1.4 Tanks	0.00	0.00	0.00	0.00	0.00
2.1.5 Cabling	0.00	0.00	0.00	0.00	0.00
2.2 ADCS					
2.2.1 Reaction Wheels	100.00	100.00	100.00	100.00	20.00
2.2.2 Inertial Measurement Unit	25.00	25.00	25.00	25.00	25.00
2.2.3 Star Tracker	16.00	16.00	16.00	16.00	16.00
2.2.4 Sun Sensor	2.50	2.50	2.50	2.50	0.00
2.2.5 Reaction Control Thrusters	27.44	27.44	27.44	54.88	0.00
2.3 Communications					
2.3.1 Traveling Wave Tube Amplifiers	233.00	233.00	0.00	0.00	0.00
2.3.2 Antennas	0.00	0.00	0.00	0.00	0.00
2.3.3 Gimbal/Motor Assembly	14.00	14.00	14.00	14.00	14.00
2.3.4 Waveguides and Coaxial Lines	0.00	0.00	0.00	0.00	0.00
2.3.5 USO	5.00	5.00	5.00	5.00	5.00
2.3.6 UHF Transceiver	71.00	71.00	71.00	71.00	71.00
2.3.7 Transponders	16.00	16.00	0.00	0.00	0.00
2.4 C&DH					
2.4.1 On-board Processor	10.00	10.00	10.00	5.00	2.50
2.4.2 Flash Memory Array	2.40	2.40	2.40	0.00	0.00
2.4.3 Crystal Oscillators	4.80	4.80	4.80	4.80	4.80
2.5 Power					
2.5.1 Solar Panel Cells	0.00	0.00	0.00	0.00	0.00
2.5.2 Batteries	0.00	0.00	0.00	0.00	0.00
2.5.3 PMAD	32.55	32.55	32.55	32.55	32.55
2.5.4 Wiring	0.00	0.00	0.00	0.00	0.00
2.6 Structure	0.00	0.00	0.00	0.00	0.00
2.7 Thermal Control	0.00	0.00	0.00	0.00	0.00
Contingency	10.00%	10.00%	10.00%	10.00%	10.00%
3.0 Total Power Required	6196.33	694.80	422.50	5865.33	209.94
4.0 Margin (25%)	25.00%	25.00%	25.00%	25.00%	25.00%
5.0 Total Power Available	7745.41	868.50	528.12	7331.67	262.42

Thermal Systems

Near Deimos, temperatures can be as low as 220 K (-53.15°C) [39]. It is crucial that the temperatures of DREAD's instrumentation be kept within their operating temperature range to prevent premature failures, as can be seen in Table 5. For this reason, DREAD will be covered in multilayer insulation (MLI) designed to minimize heat losses due to radiation and protect the instrumentation from the outside thermal environment.

Table 5. Operating temperatures for payload instrumentation.

Instrument	Operating Temperatures (K)
Camera	243.15 to 313.15
VIR detector	155 K
LIDAR	268.15 to 303.15
Batteries	273.15 to 298.15
Computer	223.15 to 393.15

A worst-case internal heat for DREAD was generated by assuming if all of the power consumed by internal instrumentation was converted to heat. The power consumption for each of these instruments can be found in Table 4. While MLI is effective at preventing heat from escaping, a build-up of excessive heat can also be problematic. Therefore, DREAD will use radiators to release waste heat. To control the exiting heat rate, louvers will be used in combination with the radiators.

Table 6. Properties of MLI for each section of layers.

MLI Design	Region A	Region B	Region C	Region D	Region E (To Surface)
Emissivity	0.03	0.03	0.03	0.03	0.03
Absorptivity	0.03	0.03	0.03	0.03	0.03
Thermal conductivity (mW/m-K)	20	20	20	20	20
Number of layers	20	10	5	3	2
Temperature (K, Louvers open)	251.79	237.66	229.11	223.18	218.72
Temperature (K, Louvers closed)	279.58	282.47	283.76	284.43	284.79
Heat leak (mW/m ² , Louvers open)	62.5	62.5	62.5	62.5	62.5
Heat leak (mW/m ² , Louvers closed)	-22.8	-22.8	-22.8	-22.8	-22.8

The 40 sheets of the MLI will be composed of double sided mylar given its low emissivity and low absorptivity [40]. As seen in Table 5, its thermal conductivity is 20 mW/m². The radiators will be composed of aluminum alloy 6061 given its high thermal conductivity and good weldability. The radiators' surfaces will be covered in silver teflon given its high emissivity as seen Table 7.

The chosen internal temperature of DREAD is 273.15 K (0°C). This is within or close to the ranges of operating temperatures of most of the on-board instrumentation. Furthermore, the TCS must be capable of rejecting at least 265 W of heat. All components of the TCS were designed according to these prescribed quantities. Along with this, the thermal analyses were simplified by approximating the surface area of DREAD to be sphere with radius 1.7 meters, which would yield a worst-case heat rate.

Table 7. Radiator properties.

Radiator Design	Value
Thermal Safety Factor	1.2
Surface Temperature (K, BOL)	291.43
Surface Temperature (K, EOL)	321.80
Emissivity	0.78
Absorptivity (BOL)	0.08
Absorptivity (EOL)	0.38
Total heat dissipation (W, BOL)	381.25
Total heat dissipation (W, EOL)	566.78
Thermal conductivity (W/m-K)	170
Total Surface Area (m ²)	1.2
Average Length (m)	1.095
Thickness (mm)	10

To account for fluctuations in the internal heat, a thermal safety factor was implemented such that the radiators' maximum heat rejection is 318 W which exceeds the total 265 W dissipated by the electronics. The radiators were then sized according to this maximum heat rejection. The MLI was designed using Lockheed Martin's MLI design optimization method [41]. The louvers' design is based on Mariner II [42].

Table 8. Louver properties.

Louver Design (Emulated MA II)	Value
Effective emissivity closed	0.08
Effective emissivity open	0.72
Blade thickness (mm)	20
% emittance when open	92.30%

Spacecraft Structure

For any launch vehicle capable of carrying the spacecraft, the maximum g-force at launch is anticipated to be five times DREAD's weight. To account for this, the solar panel booms were composed of redundant structural supports that were designed to not only hold this weight but keep their stresses within a margin specified by a structural factor

of safety (FOS) of 1.75. Typical FOSs for the aerospace industry are between 1.5 and 2, with 2 commonly used for untested vehicles [43]. The supports were sized according to the bending stresses they would experience at 5g and if the solar panels were fully extended. This was done for the following reasons. Firstly, the most stress intensive configuration of the spacecraft for the supports would be one where the solar panels were fully open. Secondly, the bending stresses were determined to be higher than any stress in the solar panel supports. The actual configuration of the spacecraft when in the payload fairing is one where the solar panels are completely closed such that it is capable of properly fitting in the fairing.

Table 9. Solar panel boom design.

Number of Boom Supports	4
Support Cross Sectional Area (m^2)	0.00962
Total Mass (kg)	0.157
Yield Factor of Safety	1.75

Table 10. Aluminum alloy 6061 T6 properties.

Young's Modulus (GPa)	68
Yield Stress (MPa)	241
Shear Modulus (GPa)	26
Shear Strength (MPa)	207

Table 11. Spacecraft bus design.

Number of plates	6
Bus Surface Area (m^2)	55.74
Bus Mass (kg)	86.11
Honeycomb Core Thickness (mm)	2
Carbon Face Plate Thickness (mm)	0.435
Total Plate Thickness (mm)	2.87
Yield Factor of Safety	1.75

For further validation of the sizes, the following requirements were to be satisfied: maximum tensile/compressive stress less than the tensile/compressive yield stress divided by the factor of safety, maximum bending stress equal to the tensile/compressive yield stress divided by the factor of safety, maximum shear stress less than the ultimate shear stress divided by the factor of safety. Analysis of the loads was done by assuming the structural supports to be circular beams with total point load equal to the weight of the solar panels. It was decided that these supports will be made of aluminum alloy 6061 T6 given its low density and high modulus of elasticity.

To account for solar and cosmic radiation, proper radiation shielding is necessary. Also, to minimize mass, a thick hull was only given to the electronics rather than giving the entire spacecraft bus thick walls. Each of the instrumentation on DREAD was given 5-millimeter-thick aluminum alloy 6061 T6 shielding. While this is very thick and adds much more weight to the spacecraft, it is necessary to protect the spacecraft's sensitive instrumentation.

For the design of the spacecraft bus, the plates of the bus were composed of carbon-aluminum honeycomb sandwiches with their cores being aluminum 5052 H39 honeycomb and their faces being T-300 carbon fiber reinforced epoxy. The aluminum honeycomb was primarily chosen for its lightweight [44] while the carbon epoxy was chosen for extremely high strength to weight ratio [45] all of which can be seen in Table 13. The thickness of the plates was determined using a similar method to how the solar panel booms were designed. However, an alternative spacecraft configuration was employed for this analysis with the plates being sized such that they can support both their own weights and the weights of the solar panels when they vertically loading the surface. More specifically, when the solar panels are down and essentially flush with the surface of the spacecraft's bus.

Table 12. Aluminum 5052 H39 honeycomb properties.

Young's Modulus (GPa)	56.5
Yield Stress (MPa)	227.5
Density (kg/m^3)	98

Table 13. T-300 Carbon fiber reinforced epoxy properties.

Young's Modulus (GPa)	138
Density (kg/m^3)	1550

Mass Budget

Each subsystem lead was responsible for the masses of the components and overall mass of their respective subsystems. However, particular care was given to the masses of the science payload and propulsion system. The chosen mode of propulsion was solar electric propulsion (SEP), as opposed to more commonly used chemical propulsion. While both systems can be seen as just as complex in their respective physics and system design, chemical propulsion requires a much greater amount of mass as opposed to SEP. Because of the low gravity conditions in space there is no gravitational gradient to drive the flow of liquid fuel thus a gaseous pressurant is needed to drive fluid flow through the propulsion system. Therefore, one must add the weight of gaseous pressurant and the tanks to store the pressurant

along with the weight of the fuel and the weight of its own tank not also forgetting the weight of piping for the fluid travel. This would only give a lower bound on the mass of the propulsive system as mass could potentially increase as one designs for undesirable factors like friction in the pipes.

These issues with mass for chemical propulsion systems are essentially entirely absent with an SEP system. DREAD's chosen propulsion engine is NASA's Evolutionary Xenon Thruster (NEXT) which is specifically an electric ion propulsion system. For electric ion propulsion system, the only fuel is gas, meaning significantly lighter weight as opposed to liquid fuel and possibly even less tank weight. Also, there is no need for pipes which means no substantial issues with friction or other undesirables that come with fluid flow through piping. Lastly, the gas is essentially its own pressurant.

For the payload, extensive science research was done by analyzing the masses of both the OSIRIS-Rex and Hayabusa missions. Initial estimates of payload masses were obtained by assuming the masses of some of the instrumentation to be percentages of the dry mass of either of the spacecraft. Extensive research was then done to obtain more accurate estimates for the masses of each of our instrumentation and drastically decrease the mass associated with each.

A contingency of 10% was given to every subsystem component. Accounting for some other factors, this yields a loaded mass of 1261 kg. For the total launch vehicle (LV) capacity, it was sized according to our LV C3, obtained from a trajectory analysis. DREAD C3 was determined to be less than $12 \text{ km}^2/\text{s}^2$ and given that the mission is in the low performance class this yield an LV capacity of 2300 kg. With all these things accounted, this yields a margin of 41.04%. The complete mass budget can be found in Table 14.

Table 14. Mass budget shows a reduced launched mass as a result of Solar Electric Propulsion.

	CBE (kg)	Level 3 Contingency	Allocated (kg)	Level 2 Subtotal (kg)	Level 1 Total (kg)
1.0 Payload					77.17
1.1 Science Instruments					43.89
1.1.1 Visible Light & IR Spectrometer	17.80	10%	19.58		
1.1.2 LIDAR	21.40	10%	23.54		
1.1.3 Dust Monitor	0.70	10%	0.77		
1.2 Cameras					13.47
1.2.1 Detector	0.25	10%	0.275		
1.2.2 Optics and Electronics	12.00	10%	13.2		
1.3 Impactor					19.8
1.3.1 Copper Lining	2.50	10%	2.75		
1.3.2 Propellant	4.50	10%	4.95		
1.3.3 Electronics and Structure	11.00	10%	12.1		
2.0 Spacecraft Bus (dry)					626.81
2.1 Propulsion					93.01
2.1.1 Thrusters	26.69	10%	29.36		
2.1.2 Gimbal	13.34	10%	14.67		
2.1.3 Power Processing Unit	19.18	10%	21.10		
2.1.4 Tanks	24.59	10%	27.05		
2.1.5 Cabling	0.75	10%	0.83		
2.2 ADCS					38.49
2.2.1 Reaction Wheels	18.00	10%	19.80		
2.2.2 Inertial Measurement Unit	4.60	10%	5.06		
2.2.3 Star Tracker	6.00	10%	6.60		
2.2.4 Sun Sensor	3.75	10%	4.13		
2.2.5 Reaction Control Thrusters	2.64	10%	2.90		
2.3 Communications					118.32
2.3.1 Traveling Wave Tube Amplifiers	12.10	10%	13.31		
2.3.2 Antennas	22.56	10%	24.82		
2.3.3 Gimbal/Motor Assembly	45.00	10%	49.50		
2.3.4 Waveguides and Coaxial Lines	8.30	10%	9.13		
2.3.5 USO	1.70	10%	1.87		

2.3.6 UHF Transceiver	11.50	10%	12.65	
2.3.7 Transponders	6.400	10%	7.04	
2.4 C&DH				1.32
2.4.1 On-board Processor	0.55	10%	0.61	
2.4.2 Flash Memory Array	0.45	10%	0.50	
2.4.3 Crystal Oscillators	0.20	10%	0.22	
2.5 Power				216.52
2.5.1 Solar Panel Cells	113.81	10%	125.19	
2.5.2 Batteries	23.60	10%	25.96	
2.5.3 PMAD	37.98	10%	41.78	
2.5.4 Wiring	21.45	10%	23.60	
2.6 Structure				112.33
2.6.1 Plates	86.10	10%	94.71	
2.6.2 Solar Panel Supports	0.16	10%	0.17	
2.6.3 Impactor Clamps	0.00	10%	0.00	
2.6.4 Camera Radiation Shielding	0.49	10%	0.54	
2.6.5 LIDAR Radiation Shielding	8.57	10%	9.42	
2.6.6 VIRS Radiation Shielding	6.80	10%	7.48	
2.7 Thermal Control				53.87
2.7.1 MLI	15.61	10%	17.17	
2.7.2 Radiators	32.40	10%	35.64	
2.7.3 Louvers	0.96	10%	1.056	
3.0 Spacecraft Dry Mass				711.02
4.0 Consumables				0.00
5.0 Propellant				550.10
6.0 Loaded Mass				1261.12
7.0 Kick Stage				0.00
8.0 Injected Mass				1261.12
9.0 Launch Vehicle Adapter				95.00
10.0 Boosted Mass				1356.12
11.0 Margin (41.04%)	41.04%			943.88
12.0 Total LV Capacity				2300.00

Software and Onboard Computing

DREAD's command and data handling subsystem needs to have sufficient computing power to match the instruments' combined data collection rate and store necessary information between each downlink period. About 85 GB of data will be downlinked per year over a total of approximately 90 downlink periods per year, leading to a required science data storage space of just under 1 GB per pass. This requirement is not difficult for modern day computers to meet, so DREAD instead focuses on implementing a high reliability onboard computing system. The BAE Systems Electronics RAD750 3U flight computer was selected as the main processor. This option is lightweight at under 1 kg of mass and is radiation hardened for increased durability in space applications. The RAD750 has been used in over 150 space missions and has a long-established flight heritage [46]. Similarly, the MIL-STD-1553C data bus architecture chosen has seen common use in American commercial and military use.

The block diagram schematic of the C&DH system, based off of the architecture used in MESSENGER, is shown in Figure 11. The architecture here is a centralized topology, and the computer has branching connections to all component subsystems, including ADCS, comms, power, and science instruments. The RAD750 communicates with these subsystems through control blocks such as the power distribution unit and data processing unit. Many reliability measures have been put into place. DREAD uses two buses and two bus controllers for redundancy to decrease the likelihood of system communication failure.

The onboard computing system is not entirely composed of the main flight computer. Some additional components to supplement the RAD750 include the oven-controlled crystal oscillators (OCXOs), secondary processor, and flash memory array. The two Q-Tech QT-4100 OCXOs serve as frequency counters to ensure the computer's clock speed remains consistent and that data is transmitted at the intended frequencies [47]. The secondary processor uses the VxWorks fault protection software, not implementable on a standard RAD750, for fault detection, isolation, and recovery procedures [48]. It receives inputs from the bus monitor, temperature sensors, and instruments

and can relay commands to the main processor if there are any anomalies. Finally, the Intel X25-E Extreme SATA Solid State Drive is a flash memory array used as a memory upgrade. Although 256 Gb of storage will exceed the size of health and instrument data many times over, a memory array of this size is relatively cheap and still small. This additional space allows DREAD to change its communications schedule later if problems arise without fear of computer limitations, and it means information can comfortably be stored if downlink malfunctions occur.

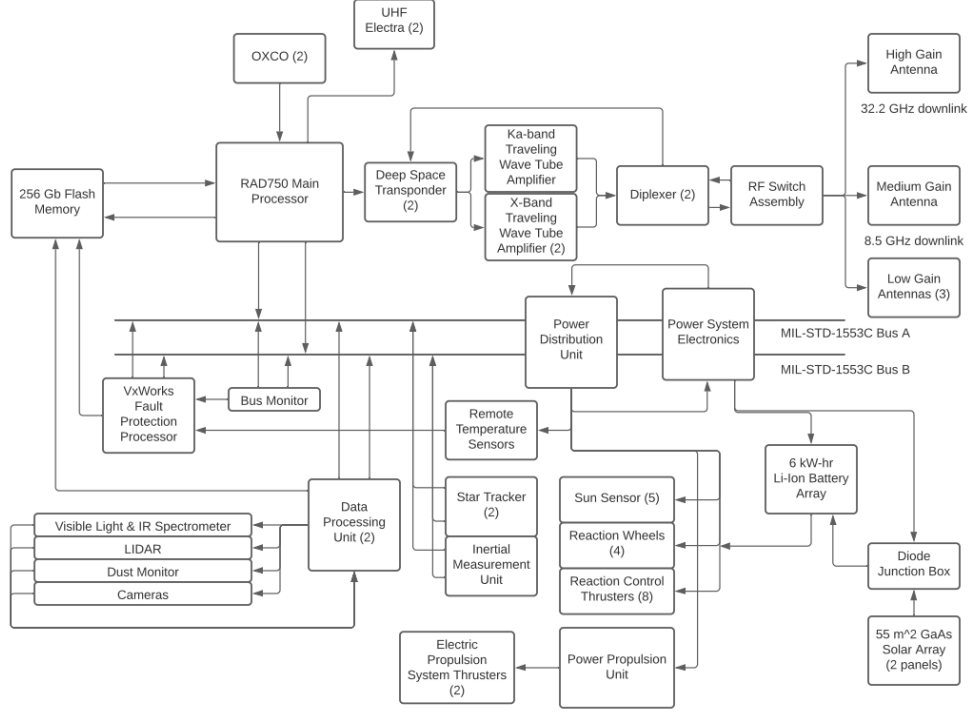


Figure 11. The block diagram organization of the C&DH system details important connections to other subsystems.

Communications

In order to support communications with Earth for both science data downlink and telemetry, DREAD will have three types of antennas. There will be one High Gain Antenna, that will be utilizing Ka-Band to downlink science data to earth, and support (but not be expected to be utilized for) X-band data uplink. There will be one Medium Gain Antenna, that will be utilizing X-band to uplink and downlink data, but it is only expected to be used if in emergency mode. And lastly, there will be three Low Gain Antennas, that will be utilizing X-Band to support telemetry uplink and downlink.

The High Gain Antenna is a parabolic antenna with a 2.4-meter diameter dish. More information about the specifics of the High Gain Antenna design can be found in Table 15, specifically regarding downlink. While there will be support for data uplink in the High Gain Antenna through X-band, this is not the intended use of this device and will only be used in the case that all other antennas no longer are feasible. The data downlink rates are reflected in the supported bandwidth range for this antenna, as for preliminary design, the bandwidth of the antenna was assumed to be equivalent in Hz to twice what the data rate would be in bits per second, as is typical for a BPSK scheme.

The Medium Gain Antenna is a fan beam antenna with a 0.2-meter diameter dish, like the medium gain antenna used in MESSENGER [49]. More information about the specifics of the Medium Gain Antenna design can be found in Table 15 and Table 16. This antenna is only intended to be utilized in emergency mode. Should there be a situation where the spacecraft is unable to point properly or determine its orientation to send data, this antenna can be used. The spacecraft will locate the sun, then rotate the medium gain antenna, while transmitting data. The moment during the rotation that the Earth receives a peak in data is how the antenna will determine its pointing to send the data down. This smaller antenna was chosen over the High Gain antenna due to the ease to move it. The data downlink rates are reflected in the supported bandwidth range for this antenna, as for preliminary design, the bandwidth of the antenna was assumed to be equivalent in Hz to twice what the data rate would be in bits per second.

The three Low Gain Antenna are choke ring horn antennas. More information about the specifics of the Medium Gain Antenna design can be found in Table 15 and Table 16. This design was chosen due to its heritage in other NASA missions such as Juno (for deep space applications) [50] and SWOT [51], and its successful usage in both. This antenna will be used to downlink and uplink telemetry data to the spacecraft, such as health data and trajectory corrections, through the utilization of X-band. Three antennas were chosen to provide increased coverage (compared to just 1) and additionally have redundancies in case one of the antennas fails. The data downlink rates are reflected in the supported bandwidth range for this antenna, as for preliminary design, the bandwidth of the antenna was assumed to be equivalent in Hz to what twice the data rate would be in bits per second.

In addition to these antennas, additional communication elements include two UHF Electra devices (for redundancy) provided for relay support for future Mars surface missions, three TWTAs (one Ka-band, two X-band for redundancy), two SDST (for redundancy), and two diplexers (one for the HGA and one for the MGA and three LGA), as similar to the mechanisms utilized for the Mars Reconnaissance Orbiter.

Table 15 and Table 16 below highlights some key values during the link budget analysis for the antennas. The formulas for these calculations were obtained from [52]. Any values about the transmit antenna characteristics for uplink and the receive antenna for downlink were obtained from [53] from the DSN itself. Information about the atmospheric losses were obtained from [54]. The pointing error comes from the pointing error budget that MRO utilized, as shown in [55] and the E_b/N_0 required, without considering margin, was determined from [56] for a BPSK encoding scheme and a bit error rate of 10^{-5} . For the high gain antenna, an implementation loss of 1 dB and a link margin of 6 dB were utilized, and for the medium and low gain antennas, an implementation loss of 3 dB and a link margin of 5 dB were used. This fits within the expected range of 1-3 dB for implementation loss and a link margin of 3-5 dB for X-band and 6+ dB for Ka-band.

Table 15. The antenna downlink budget parameters provide a sufficient signal-to-noise ratio.

Downlink Parameters	HGA Downlink	MGA Downlink	LGA Downlink
Frequency (GHz)	32.2	8.5	8.5
Bandwidth (kHz)	260 - 3806	0.794 - 11.04	0.052 - 0.724
Transmit Antenna Gain (dBi)	55.57	22.41	10.5
Receive Antenna Gain (dBi)	79.18	68.3	68.3
Max Space loss (dB)	-294.67	-283.1	-283.1
Atmospheric Loss (dB)	-2.28	-2.28	-2.28
Input Power (W)	232.56	232.56	232.56
Received Power (W)	1.79×10^{-15}	3.2×10^{-18}	2.2×10^{-19}
E_b/N_0 (dB)	16.69	17.62	17.86

Table 16. The antenna uplink budget parameters provide a sufficient signal-to-noise ratio.

Uplink Parameters	HGA Uplink	MGA Uplink	LGA Uplink
Frequency (GHz)	8.5	8.5	8.5
Bandwidth (kHz)	180-512	1.6-68	.11-6
Transmit Antenna Gain (dBi)	67.09	67.09	67.09
Receive Antenna Gain (dBi)	42.54	20.96	10.50
Max Space loss (dB)	-281.65	-281.65	-281.65
Atmospheric Loss (dB)	-2.28	-2.28	-2.28
Input Power (W)	20000	20000	20000
Received Power (W)	3.6×10^{-14}	2.2×10^{-16}	1.98×10^{-17}
E_b/N_0 (dB)	17.68	17.64	17.77

When looking into collecting and downlinking science data, there is a balance that needs to be achieved between time spent collecting and time spent downlinking to achieve successful collection of all necessary science data within the mission timelines. To achieve this, it was determined to collect data for three orbits, and then spend time downlinking the science data collected during that time. Each orbit is 30 hours, and during one science orbit DREAD collects approximately 0.317 GB of science data. Therefore, each downlink cycle consists of downlinking .95 GB of data. Each collect-downlink cycle will be a different time based on the distance Earth is from the spacecraft, and the resultant length of each data collect-downlink cycle is shown in Figure 12 for Stage B orbits and Figure 13 for Stage C orbits. For Stage B orbits, the longest downlink time is 16.3 hours, and this consists of 11.5% of the time in orbit is spent downlinking, for a total of 86 cycles. For Stage C orbits, the longest downlink time is 15 hours, and this consists

of 7.3% of the time in orbit is spent downlinking, for a total of 90 cycles. Therefore, DREAD can collect 81.7 GB of data during Stage B orbits and 85.5 GB of data during Stage C orbits.

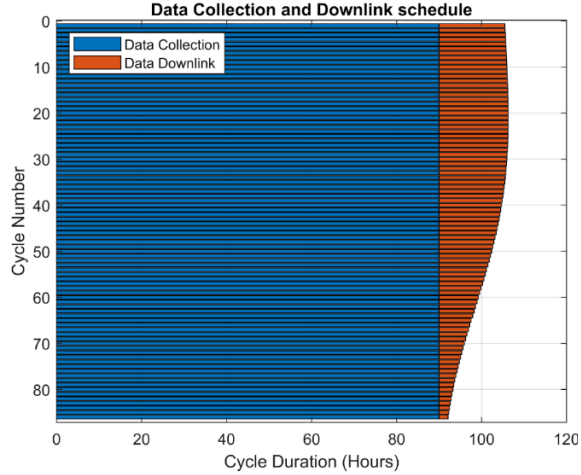


Figure 12. In Stage B, DREAD's HGA can transmit its science data back to Earth in a very short amount of time relative to collection time.

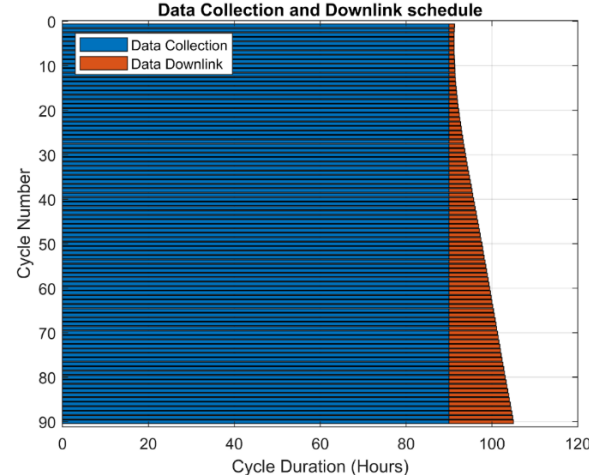


Figure 13. Deimos' favorable location in Stage C orbits, reduces science data transmission time over the one-year collection period.

Spacecraft and Mission Visualization

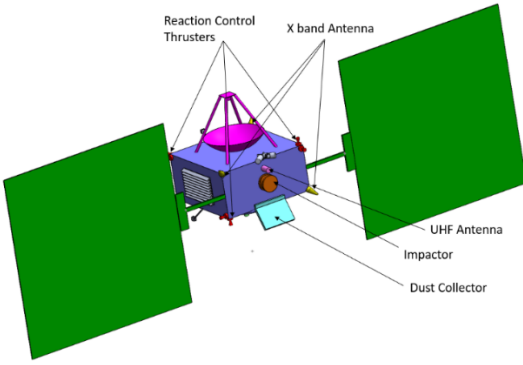


Figure 14. X-Band Antennae are placed on three opposing faces of the spacecraft to improve the line of sight while the solar arrays are deployed.

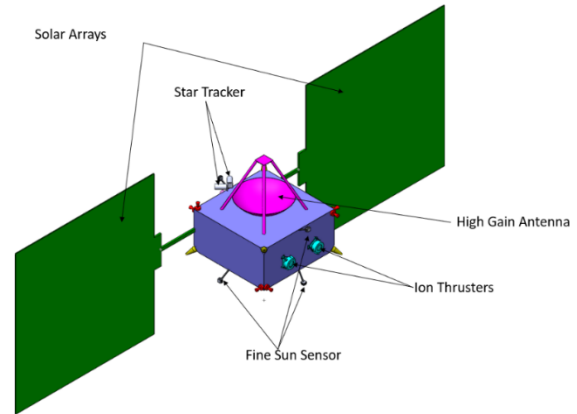


Figure 15. Ion thrusters are mounted at a 90-degree angle to both the instrument deck and the high gain antenna to avoid conflicting attitude requirements.

The DREAD spacecraft utilizes a main primary structure that is $2.54 \times 2.52 \times 1.7 \text{ m}^3$ in volume. Due to DREAD's Solar Electric Propulsion system, the spacecraft's solar arrays have a total area of 55.25 meters-squared to provide a total of 8.5 kW of power during its long duration burns. The top face of the primary structure is largely occupied by the communication system's high gain antenna to make sure it's field of view is not restricted by any instruments. The impactor used for Stage C of DREAD's mission occupies the forward face of the spacecraft to reduce the required attitude change during its deployment.

The spacecraft's eight reaction control thrusters are configured into four clusters of two units to allow for at least one pair of thrusters to provide actuation about the spacecraft's three rotational degrees of freedom. Each fine sun sensor is attached to a secondary support structure that extends beyond the surface of the primary structure to improve the unit's field of view. As mentioned previously, the two ion thrusters are attached to a gimbaling system allowing them to rotate independently of the spacecraft during long duration burns.

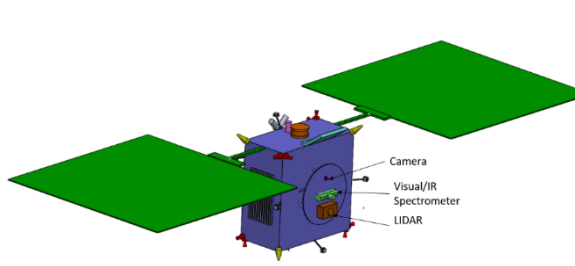


Figure 16. DREAD's three science instruments are mounted onboard the main instrument deck to isolate an oscillation made by the spacecraft bus.

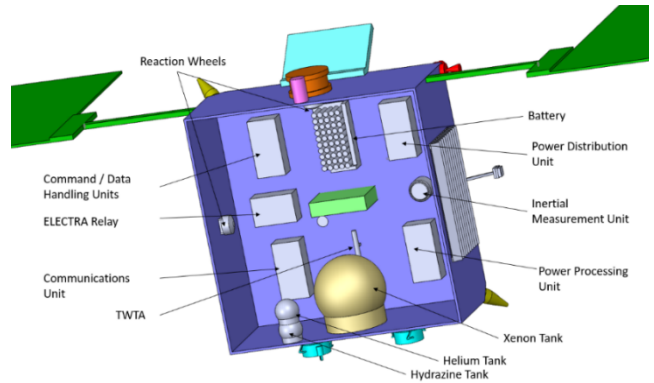


Figure 17. DREAD's interior volume is more than sufficient for storing components needed for managing the electric propulsion system, command and data handling, as well as communications equipment.

Due to the use of solar electric propulsion, the volume occupied by propellant for both the main propulsion systems and the reaction control thrusters is very small compared to the total interior volume. This allows the spacecraft's components to be enclosed within the spacecraft where the thermal environments of each component can be managed by DREAD's thermal control system. Interior components were modelled either using parameters provided within their specifications (such as the IMU and reaction wheels), reference components with similar parameters (such as the battery), or conservative estimates of their total bounding volume (such as the communications, and C&DH Units). The PPU dimensions were based off APL's DART mission which utilized the same NEXT-C Propulsion System [57]. The xenon, hydrazine, and helium pressurant tanks were all sized based of the requirements of the ADCS and trajectory subsystems.

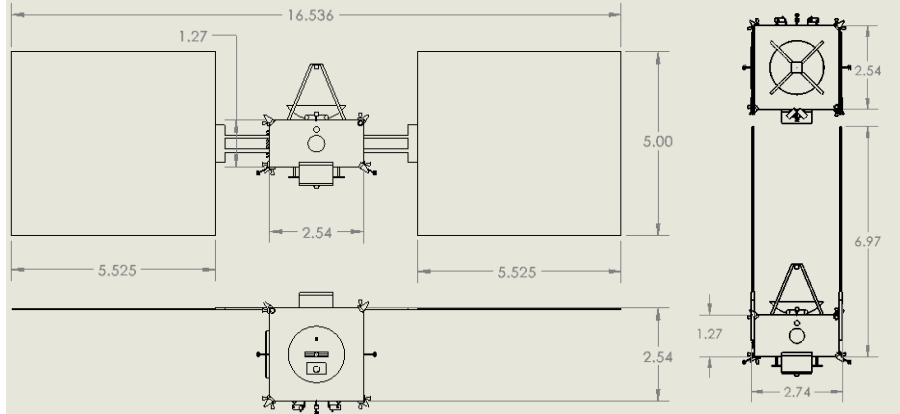


Figure 181. With the solar arrays in their stowed configuration, DREAD is capable of fitting inside both the medium and large fairings of the Atlas V launch vehicle.

Prior to launch vehicle integration, DREAD's two solar arrays will be configured to allow the spacecraft to fit within the payload fairing volume. This is done by separating each array into two segments which will be able to rotate by 90 degrees in addition to the main support structure folding similarly so the length of the array is pointed towards the top of the fairing. Upon deployment from DREAD's launch vehicle, DREAD will deploy its two solar arrays into the configuration seen in the figures above. The solar arrays are attached to two structures that support the underlying substrate in addition to separate the arrays from the primary structure to avoid the closer segments of the arrays from being in the structure's shadow. Figure 18 shows the DREAD spacecraft in both the deployed and stowed formation. You can see from the stowed configuration that the main spacecraft bus as well as the solar arrays are capable of fitting within vehicles that utilize either a four- or five-meter fairing. This, in addition to the mission's low

C3 requirement, makes DREAD compatible with a large variety of launch vehicles that will be available during its 2026 launch window.

Data Management and Archiving

Once DREAD has collected, and transmitted data towards Earth, ground stations of the Deep Space Network will receive data and transmit it to DREAD's mission operation center. This data will then be transmitted to the mission science teams for processing and analyzing the spacecraft's raw data. [58]

The processed data will then be transformed into Planetary Data System (PDS) compatible file formats. The PDS is NASA's archiving system, which will allow for the storage of DREAD's data. Once each file has a format approved by the PDS, it will be named in a form describing the structure and content of the data file. Should any additional information be needed to interpret the data, it will be provided as ancillary archive components. In addition, should any software be used for archive generation, it will also be collected and documented in the PDS. Finally, data will be divided into separate data set collections, one for each detector [59].

Integration and Test

As the procurement of DREAD's major components is proceeding, the procurement team will fabricate the satellite bus. Once every component is tested by vendors or contractors, a team of propulsion specialists will assemble the satellite's propulsion systems. The integration and test team will then install bus and payload electronics. When bus electronics units communicate and interact with each other as expected, auxiliary payloads (sensors, mission-specific electronics) are integrated. After an initial payload test, final components, such as solar arrays, radiators, or antennas, are integrated into the systems.

Prior to full system integration, each component will be tested individually based on its unique operating thermal and electromagnetic environments in addition to the vibration levels experienced during launch. After component level testing the spacecraft will be put through system level testing starting with the most aggressive tests such as vibration and thermal testing prior to EMI and final functional testing.

As the spacecraft integration comes to an end, the satellite must be tested to withstand the extremes of space. Therefore, it must satisfy the General Environmental Verification Standard (GEVS) for Goddard Space Flight Center (GSFC) Flight Programs and Projects. This standard applies to all space flight hardware developed as part of a payload managed by NASA [60]. Table 17 below lists the tests and descriptions DREAD will have to satisfy for launch. These will be performed by the project's primary contractor and may also be performed using software beforehand to approximate the spacecraft's performances.

Table 17. The tests performed on DREAD will ensure that the mission successfully operates on-orbit.

Name	Description
Thermal vacuum test	The satellite is placed in a chamber which is pumped down to near-vacuum conditions. The temperature of the chamber is then varied between extremely cold and hot (typically between 180°C to -200°C, over the course of several days).
Electromagnetic interference and electromagnetic compatibility test	The satellite is powered up and the amount of electromagnetic energy each component is producing is tabulated to ensure no device on the satellite is emitting significant amounts of electromagnetic energy, which could interfere with the satellite's proper operation.
Vibration test	Simulates launch induced vibration and vibration caused by the propulsion system to ensure that the satellite's structure will withstand launching into space.

Risk Analysis

DREAD is a class B mission [63], which implies that the mission must maintain low risk throughout its life to achieve mission success. The risk matrix in Figure 19 and Table 18 show that some risks may have significant consequences, such as risks 1a, 1b, 2, or 3, which could cause the loss of the spacecraft or failure of the mission these tend to be unlikely. Indeed, further research will be performed to ensure risks 1a and 1b are minimized, and lessons learned from past missions help safeguard against risk 2.

Testing the spacecraft subsystems will mitigate the likelihood of risks 3, 5, and 6. Additional safety devices have also been implemented in the impactor, using solar panels instead of a switch to indicate deployment. Indeed, while switches are common to signal when equipment is separated from its mother spacecraft, it may be triggered during

turbulent phases of flight, such as during launch. While this may be harmless in most cases, wrongly arming the impactor would destroy the spacecraft. As such, the impactor is armed once light reaches its solar panels, ensuring that it cannot be armed unless it is separated from DREAD.

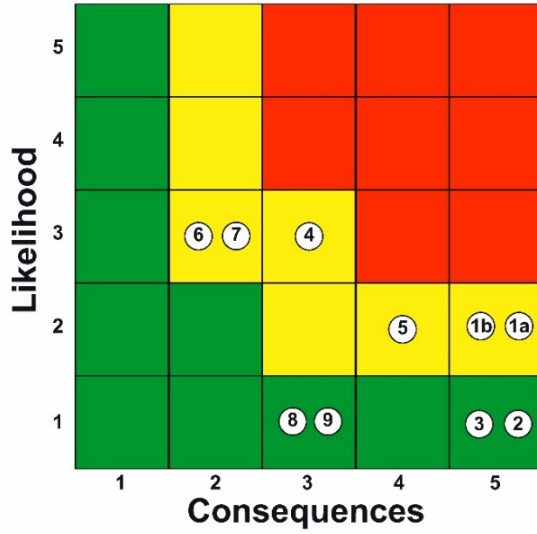


Figure 19. DREAD risk matrix: Consequences relate to the risk's impact on the spacecraft, 1 being the least.

Table 18. Risk IDs and descriptions.

ID	Risk description
1a	Failure to enter Deimos orbit due to ion engine
1b	Limited understanding of the vehicle's operational environment (Deimos-synchronous Martian orbit)
2	Solar panel deployment failure
3	In-flight activation of impactor
4	Modifications of heritage elements is not adequately accounted for in the proposal
5	Launch vehicle thrust oscillations near resonance frequency of payload
6	Stray light may enter the science package causing loss in video and image quality
7	Higher than expected development costs
8	Inadequate margins for mass
9	Dust monitor has not reached TRL 6

Numerous systems of DREAD were chosen due to their success on previous missions. However, while it was assumed that these elements would be used in the same configuration as in past missions, some heritage elements likely need to be updated to enable higher performances or modified to fulfill mission objectives. Developmental costs may rise as a result. In addition, instrumentation costs were computed from past cost trends, some of which have R2 values as low as 0.65 [64]. While this mainly implies a high spread of the data used to create a trendline and may cause estimated costs to be lower or higher, it shows relative uncertainty in the cost figures calculated.

Finally, as mass margins were calculated from past missions, it is unlikely for DREAD to exceed these margins. Nevertheless, this risk must be watched to avoid changing launch vehicles or losing additional funds. Similarly, it is also unlikely for the Circum-Martian Dust Monitor to be incomplete by the 2026 launch date, as it is currently being developed for JAXA's 2024 Martian Moons Explorer mission. However, should the instrument be unfinished by MMX's launch, DREAD has allocated resources to complete the development of a CMDM.

Management

Team roles were designated according to the Team Skills Matrix shown in Table 19. Each member was assigned to at least two subsystems and served as the lead for at least one subsystem. The breakdown of tasks was aimed to evenly divide the work among team members while ensuring that all requirements were met. In particular the Science Payload Systems Engineer, Power, Propulsion, and Thermal and Trajectory and GNC/ADCS subsystems included additional members due to the complexity associated with their respective tasks.

The roles of Principal Investigator and Project Manager were combined into a single Student Manager/PI role. The PI verified the mission's compliance with the requirements set-forth in the Announcement of Opportunity, organized team meetings, and ensured that the mission met its overall science objectives. A separate Project Systems Engineer (PSE) was designated to develop mission-level requirements, interface the subsystems, and define system trades. As shown in Figure 19, a flat team structure was chosen to streamline communications. The project work breakdown structure is detailed in Figure 22, indicating the specific instruments allocated to each subsystem.

Table 19. Team roles efficiently divided the work among members. Names are abbreviated to first and last initials.

Team Member	JC	BJ	NL	CL	GM	KR	JS	ST	AZ
Student Manager/PI									L
Project Systems Engineer (PSE)			L						
Science Payload Systems Engineer				x	x		x		L
Communications		x						L	
Trajectory and GNC/ADCS	x	x				L			x
Power, Propulsion and Thermal			x		L	x		x	
Structures and Mass Properties					L			x	
Software and Onboard Computing								L	
Spacecraft & Mission Visualization		L		x					
Ground Systems and Operations				L					
Spacecraft Integration and Testing		L		x					
Schedule and Cost						L		x	

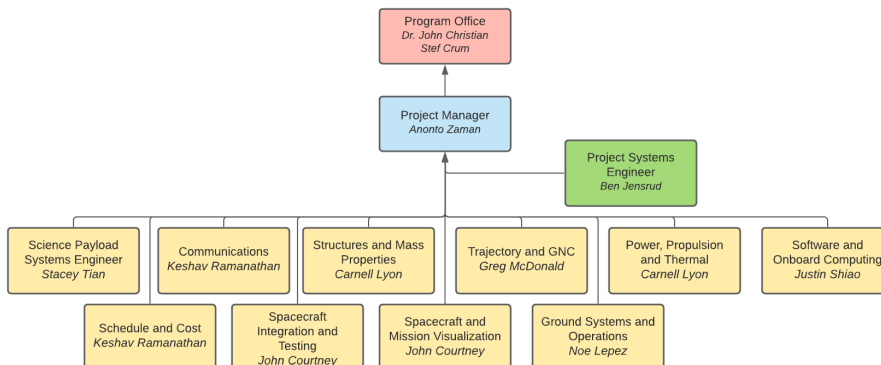


Figure 20. The team structure is flat to streamline communication and minimize overhead.

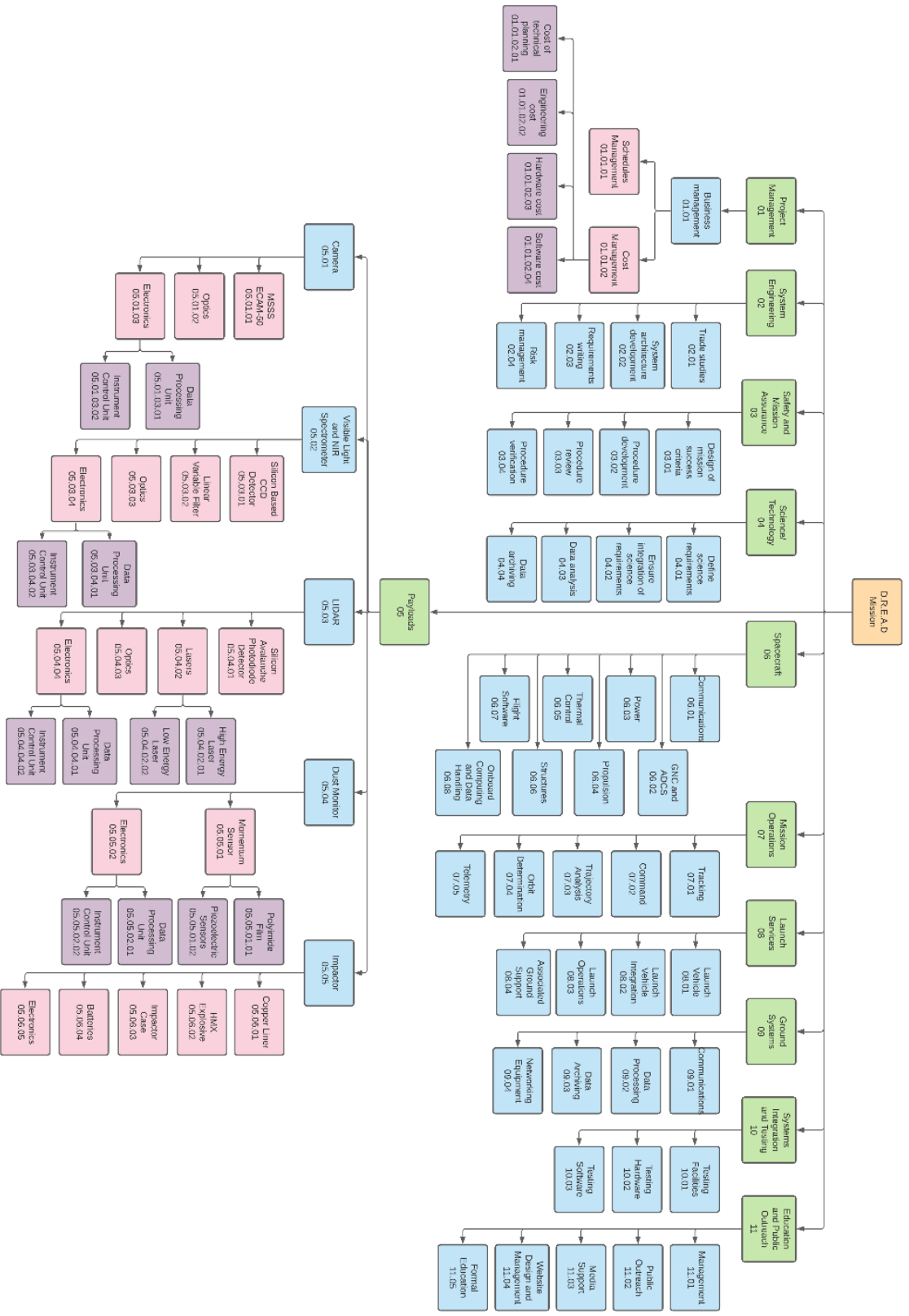


Figure 21. The team Work Breakdown Structure illustrates the distribution of specific tasks to each subsystem. Specific detail was added to the Payload subsystem due to its importance for the science mission.

Cost and Schedule

Gantt Chart

As with a typical NASA mission, the lifecycle will consist of six phases, A-F. Estimates for the phase duration for the mission lifecycle come from historical phase durations for previous NASA projects that consisted of a moderately complex payload with new engineering. Phase A, which consists of concept and technology development, will last from February 2022 till August 2022, with margin up to September 2022. This presents a total seven-month period, with a one-month margin. Phases A through C operate under a rounded up one-month/year margin. During this time, some of the main actions that will be performed include developing the top-level requirements, allocating, and validating them, and developing many baseline plans such as the Systems Engineering Management Plan. The two main reviews for this phase will consist of the System Requirements Review, which will happen in the middle of Phase A once the requirements allocation has been completed, and then lastly the mission definition review that will gate the phase.

Next is Phase B, which consists of preliminary design and technology completion. This period will last for seven months, from October 2022 to April 2023, with a one-month margin to May 2023. The main tasks are developing the preliminary design, developing the operations plan, and identifying new and updating risks for the mission. The gate for this phase will be the Preliminary Design Review, which is tentatively scheduled for the end of April 2023.

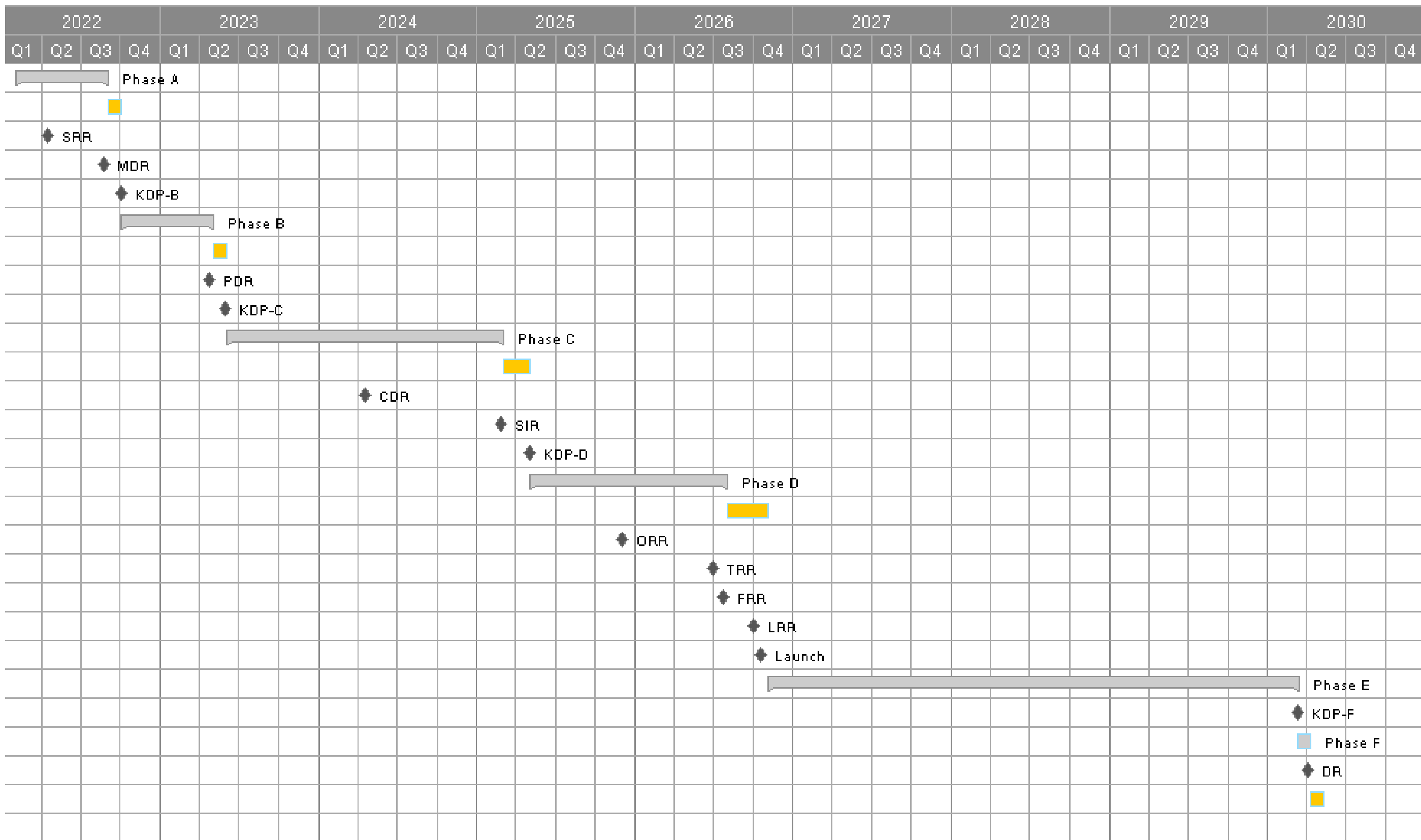
After that is Phase C, which is final design and fabrication. Some main action items in this phase will be developing the various critical procedures (ex. integration procedure), developing the communications and decommissioning plans in detail, and performing appropriate subsystem testing. This phase lasts 21 months from June 2023 to February 2025, with a margin of two months lasting in March 2025 and April 2025. The main design reviews will be the Critical Design Review, which will happen in the middle of the phase (Summer 2024), and a System Integration Review to close the phase.

Finally, the last development phase of Phase D, which is the system assembly, test, & launch. In this phase, the subsystem components will be assembled, be tested and have requirements validated, and have the launch and ground support sites properly prepared for the scheduled launch. Since the potential for delays in this phase, and the proximity to launch date, this phase has a larger phase margin of approximately two-months/year. This phase lasts from May 2025 until July 2026 for a total of 15 months, with a margin of three months lasting from August 2026 to October 2026. In this phase, the system will first go through an Operational Readiness Review before going through a Test Readiness Review, Flight Readiness Review, and Launch Readiness Review before the launch date. The launch date is tentatively planned for October 17, 2026, but there is an additional margin of several weeks.

After launch begins, Phase E consists of the main system operations. Immediately after launching, a Post Launch Assessment Review will be performed. The spacecraft will then get into an appropriate trajectory to approach Mars, and then cruise until December 19, 2027 where it will enter Mars SOI. Before arriving at Mars however, the mission will undergo a Critical Events Readiness Review. Ten days after entering the Mars SOI, the spacecraft will enter the Deimos SOI, upon which it will begin the initial Stage A orbits as it spirals to its Stage B orbits. This will occur for 43 days and allow the spacecraft to get a better understanding of its environment. After that, Stage B orbits will occur for approximately one year, lasting from February 10, 2028 to February 10, 2029, to collect science data from a distance. Then, the spacecraft will take a week to get down to closer distance to release the impactor, which is currently planned to be released on February 17, 2029. After that, the spacecraft will return to a higher altitude and wait 20 days until beginning Stage C orbits, from March 10, 2029 to March 10, 2030.

Finally, starting March 11, 2030, the mission will begin decommissioning in Phase F, as it goes into a heliocentric graveyard orbit. There is currently one month budgeted for this to occur, with one month for margin, but this margin and time also serves as a margin to the mission life for Phase E. Finally, after decommissioning activities have been completed, there will be a Decommissioning Review to complete the system life.

Figure 22. The DREAD mission will launch by the end of 2026 and perform its complete science mission during the next 3.5 years.



Cost Tables

The DREAD mission will have a PI-Managed Mission Cost of FY21 \$482,295,857 or RY \$517,703,671, and a Total Mission Cost of FY21 \$483,913,216. Since DREAD will be using a Low Performance Class launch vehicle, owing to its low mass and C3, the Adjusted AO Cost Cap of FY21 \$515M is applicable. Prior to KDP-C, FY21 \$112,721,590 or 23.35% of the PI-Managed Mission Cost will be incurred. Furthermore, during every phase, the planned unencumbered cost reserves are equal to 25% of the cost to complete each respective phase. A full budget for phases A through E of DREAD is provided below as Table 20.

Total costs for each subsystem in FY 2010 dollars were calculated using the USCM8 CER [65], NICM CER [66], and wrap factors [67] provided in SME-SMAD. Since DREAD will be using a solar electric propulsion system, a separate cost model developed by Hofer and Randolph was used [68], providing costs in FY 2013 dollars, which were subsequently deflated to FY 2010 dollars for consistency with SME-SMAD values. The resulting values were then inflated using the appropriate inflation factors from SME-SMAD to FY 2021 dollars [69].

Firstly, the non-reoccurring and reoccurring costs for the spacecraft bus were calculated using the USCM8 CER and the SEP cost model. Each CER is primarily mass driven and thus the cost driver that was inputted into each equation was the allocated mass for a given subsystem. Since the WBS elements presented in SME-SMAD are not the same as the NASA WBS elements, the CER for Telemetry, Tracking, and Command used the mass of C&DH as well as communications (minus the government furnished Electra payload mass). The Electra payload mass was temporarily included to calculate the Total Mission Cost. To allocate this single cost between the two subsystems, mass ratios were used. No money was assigned to the Flight Software WBS element as these costs are absorbed in the CERs of the other subsystems.

For the instrumentation costs, the NICM CERs were used, taking in the allocated mass, allocated power, and design life for each instrument. The camera, spectrometer, and LIDAR system fell under the Optical Planetary instrument subcategory; the dust monitor was considered a Particles Payload; and the impactor cost was calculated based on a mass fraction of the total Hayabusa2 mission cost, deflated to its FY 2010 value. NICM provided management cost CERs were then applied to the instrument cost. The other NICM provided wrap factors were not included since those costs were included in the USCM8 CERs. The NICM values were then divided up into non-reoccurring and reoccurring costs with a ratio of 2:1, which was consistent with the spacecraft bus.

Integration, assembly, and test; program level; and aerospace ground USCM8 CERs were then applied to the spacecraft bus and payload costs. To separate the program level cost between Project Management, Systems Engineering, Safety & Mission Assurance, and Science/Technology, the total program level cost was divided up between the 4 subsystems according to their average wrap factors, provided in SME-SMAD, or a ratio of 25:10:7:2 respectively [67]. Launch Vehicle/Services costs were not included since DREAD will be using standard services provided by NASA.

Finally, Mission Operations costs were estimated using a 3% wrap factor around the payload and spacecraft bus cost. The costs associated with Education and Public Outreach were defined to be 1% of the total cost and Reserves were defined to be 25% of planned costs. All values were then inflated to FY 2021 dollars to obtain the PI-Managed Mission Cost.

To spread the total subsystem costs across all the phases, the Weibull Distribution presented in SME-SMAD was used [70]. The applicable phases for each subsystem were first identified. FY 2010 costs were spread across the phases based on the total duration of each respective subsystem, the number of units, the percentage of non-reoccurring costs, and a Weibull shape factor of 1.71. Time elapsed was based on the number of months that had passed at the end of each fiscal year in each phase. The costs were then inflated using SME-SMAD provided inflation factors to their respective years to obtain real year dollar values.

Since every phase has its own built in 25% margin and many of DREAD's subsystems have previously flown on other missions and are thus at TRL 9, the actual costs are expected to be lower than predicted here. Furthermore, DREAD is also approximately FY21 \$32M below the Adjusted Cost Cap, and approximately \$17M below the Cost Cap. Thus, DREAD is projected to execute the full breadth of science, which has implications not only for Deimos but for Mars and other bodies in the Solar System, within the cost cap of a Discovery class mission.

Table 20. Budget for the PI-Managed portion of project DREAD in thousands of dollars during each phase of the mission including 25% cost margins that allows for the full breadth of science that DREAD hopes to accomplish to be achieved within the Adjusted Cost Cap.

WBS#	WBS Element	Phase A		Phase B			Phase C/D					Phase E					RY\$	FY21\$
		FY 2022	Total	FY 2022	FY 2023	Total	FY 2023	FY 2024	FY 2025	FY 2026	Total	FY 2026	FY 2027	FY 2028	FY 2029	Total	Total	Total
01	Project Management	\$3,971	\$3,971	\$2,523	\$4,976	\$7,499	\$7,560	\$12,289	\$9,249	\$5,128	\$34,226	\$776	\$3,447	\$2,030	\$950	\$7,203	\$52,899	\$49,312
02	Systems Engineering	\$1,588	\$1,588	\$1,009	\$1,990	\$3,000	\$3,024	\$4,916	\$3,699	\$2,051	\$13,690	\$310	\$1,379	\$812	\$380	\$2,881	\$21,159	\$19,725
03	Safety & Mission Assurance	\$1,112	\$1,112	\$707	\$1,393	\$2,100	\$2,117	\$3,441	\$2,590	\$1,436	\$9,583	\$217	\$965	\$568	\$266	\$2,017	\$14,812	\$13,807
04	Science/Technology	\$318	\$318	\$202	\$398	\$600	\$605	\$983	\$740	\$410	\$2,738	\$62	\$276	\$162	\$76	\$576	\$4,232	\$3,945
05	Payload(s)	\$6,315	\$6,315	\$3,958	\$7,514	\$11,471	\$10,573	\$14,680	\$8,637	\$3,763	\$37,654	\$0	\$0	\$0	\$0	\$0	\$55,440	\$52,500
05.01	Camera	\$813	\$813	\$510	\$968	\$1,477	\$1,362	\$1,891	\$1,112	\$485	\$4,849	\$0	\$0	\$0	\$0	\$0	\$7,140	\$6,761
05.02	Visible Light and IR Spectrometer	\$1,609	\$1,609	\$1,008	\$1,914	\$2,922	\$2,693	\$3,740	\$2,200	\$959	\$9,592	\$0	\$0	\$0	\$0	\$0	\$14,123	\$13,374
05.03	LIDAR	\$2,955	\$2,955	\$1,852	\$3,516	\$5,367	\$4,947	\$6,869	\$4,041	\$1,761	\$17,617	\$0	\$0	\$0	\$0	\$0	\$25,939	\$24,563
05.04	Dust Monitor	\$421	\$421	\$264	\$500	\$764	\$704	\$978	\$575	\$251	\$2,508	\$0	\$0	\$0	\$0	\$0	\$3,692	\$3,496
05.05	Impactor	\$518	\$518	\$324	\$616	\$941	\$867	\$1,204	\$708	\$309	\$3,087	\$0	\$0	\$0	\$0	\$0	\$4,546	\$4,305
06	Spacecraft	\$19,520	\$19,520	\$12,229	\$23,208	\$35,438	\$32,627	\$45,214	\$26,522	\$11,527	\$115,890	\$0	\$0	\$0	\$0	\$0	\$170,847	\$161,79
06.01	Communications	\$4,903	\$4,903	\$3,065	\$5,793	\$8,858	\$8,076	\$11,008	\$6,295	\$2,675	\$28,055	\$0	\$0	\$0	\$0	\$0	\$41,815	\$39,621
06.02	GNC and ADCS	\$2,877	\$2,877	\$1,804	\$3,431	\$5,235	\$4,841	\$6,759	\$4,010	\$1,761	\$17,371	\$0	\$0	\$0	\$0	\$0	\$25,483	\$24,127
06.03	Power	\$3,128	\$3,128	\$1,960	\$3,723	\$5,683	\$5,242	\$7,285	\$4,293	\$1,873	\$18,693	\$0	\$0	\$0	\$0	\$0	\$27,504	\$26,044
06.04	Propulsion	\$4,100	\$4,100	\$2,582	\$4,953	\$7,535	\$7,114	\$10,294	\$6,454	\$2,983	\$26,844	\$0	\$0	\$0	\$0	\$0	\$38,479	\$36,387
06.05, 06.06	Structure and Thermal Control	\$3,970	\$3,970	\$2,476	\$4,657	\$7,133	\$6,434	\$8,610	\$4,789	\$1,987	\$21,820	\$0	\$0	\$0	\$0	\$0	\$32,923	\$31,214
06.07	Flight Software	\$0	\$0	\$0	\$0	\$0	\$0	\$0	\$0	\$0	\$0	\$0	\$0	\$0	\$0	\$0	Part of other lines	
06.08	Onboard Computing and Data Handling	\$545	\$545	\$341	\$644	\$984	\$897	\$1,223	\$699	\$297	\$3,117	\$0	\$0	\$0	\$0	\$0	\$4,646	\$4,402
07	Mission Operations	\$0	\$0	\$0	\$0	\$0	\$0	\$0	\$0	\$0	\$0	\$121	\$2,410	\$3,162	\$1,740	\$7,433	\$7,433	\$6,429
08	Launch Vehicle/Services	\$0	\$0	\$0	\$0	\$0	\$0	\$0	\$0	\$0	\$0	\$0	\$0	\$0	\$0	\$0	NA	
09	Ground System(s)	\$0	\$0	\$0	\$0	\$0	\$0	\$0	\$0	\$0	\$0	\$1,019	\$19,164	\$16,867	\$5,443	\$42,492	\$42,492	\$36,944
10	Systems Integration & Testing	\$0	\$0	\$0	\$0	\$0	\$5,263	\$16,388	\$12,607	\$5,402	\$39,660	\$0	\$0	\$0	\$0	\$0	\$39,660	\$36,874
11	Education and Public Outreach	\$0	\$0	\$0	\$0	\$0	\$747	\$2,244	\$1,584	\$610	\$5,185	\$0	\$0	\$0	\$0	\$0	\$5,185	\$4,827
	Reserves	\$8,207	\$8,207	\$5,157	\$9,868	\$15,025	\$15,623	\$25,030	\$16,411	\$7,594	\$64,659	\$626	\$6,910	\$5,900	\$2,214	\$15,651	\$103,541	\$96,539
	PI-Managed Mission Cost																\$517,704	\$482,69

References

- [1] Zurbuchen, T. H., “Mars Exploration Program,” National Academies Available: https://sites.nationalacademies.org/cs/groups/ssbsite/documents/webpage/ssb_181241.pdf.
- [2] Duxbury, T. C., Zakharov, A. V., Hoffmann, H., and Guinness, E. A., “Spacecraft exploration of Phobos and Deimos,” Planetary and Space Science, vol. 102, Nov. 2014, pp. 9–17. <https://doi.org/10.1016/j.pss.2013.12.008>
- [3] Deimos, National Aeronautics and Space Administration, Available: <https://mars.nasa.gov/all-about-mars/moons/deimos/>
- [4] Campagnola, S., Yam, C. H., Tsuda, Y., Ogawa, N., and Kawakatsu, Y., “Mission analysis for the Martian Moons Explorer (MMX) mission,” Acta Astronautica, vol. 146, Mar. 2018, pp. 409–417. <https://doi.org/10.1016/j.actaastro.2018.03.024>
- [5] Murchie, S. L., Britt, D. T., and Pieters, C. M., “The value of Phobos sample return,” Planetary and Space Science, vol. 102, Nov. 2014, pp. 176–182. <https://doi.org/10.1016/j.pss.2014.04.014>
- [6] Hartmann, W. K., “Additional evidence about an early intense flux of C asteroids and the origin of Phobos,” Icarus, vol. 87, Sep. 1990, pp. 236–240. [https://doi.org/10.1016/0019-1035\(90\)90033-6](https://doi.org/10.1016/0019-1035(90)90033-6)
- [7] Deutsch, A. N., Head, J. W., Ramsley, K. R., Pieters, C. M., Potter, R. W., Palumbo, A. M., Bramble, M. S., Cassanelli, J. P., Jawin, E. R., Jozwiak, L. M., Kaplan, H. H., Lynch, C. F., Pascuzzo, A. C., Qiao, L., and Weiss, D. K., “Science exploration architecture for Phobos and Deimos: The role of Phobos and Deimos in the future exploration of Mars,” Advances in Space Research, vol. 62, Oct. 2018, pp. 2174–2186. <https://doi.org/10.1016/j.asr.2017.12.017>
- [8] Burns, J. A., “Some Background About Satellites,” Satellites, 1986, pp. 1–38.
- [9] Craddock, R. A., “Are Phobos and Deimos the result of a giant impact?,” Icarus, vol. 211, Feb. 2011, pp. 1150–1161. <https://doi.org/10.1016/j.icarus.2010.10.023>
- [10] SBAG (2020), Goals and Objectives for the Exploration and Investigation of the Solar System’s Small Bodies. ver. 2.0.2020, 44 p., at <http://www.lpi.usra.edu/sbag/goals/>
- [11] Pratt, W., and Hopkins, J., “Comparison of Deimos and Phobos as Destinations for Human Exploration and Identification of Preferred Landing Sites,” AIAA SPACE 2011 Conference & Exposition, Sep. 2011. <https://doi.org/10.2514/6.2011-7140>
- [12] Deimos and Phobos Orbit, Planetary Science, Available: <https://planetary-science.org/mars-research/moons-of-mars/>
- [13] Zakharov, A., Horanyi, M., Lee, P., Witasse, O., and Cipriani, F., “Dust at the Martian moons and in the circummartian space,” Planetary and Space Science, vol. 102, Nov. 2014, pp. 171–175. <https://doi.org/10.1016/j.pss.2013.12.011>
- [14] Takir, D., Matsuoka, M., Waiters, A., Kaluna, H., and Usui, T., “Observations of Phobos and Deimos with SpeX at NASA infrared telescope facility,” Icarus, vol. 371, Jan. 2022, p. 114691. <https://doi.org/10.1016/j.icarus.2021.114691>
- [15] Thomas, P. C., Adinolfi, D., Helfenstein, P., Simonelli, D., & Veverka, J. (1996). The Surface of Deimos: Contribution of Materials and Processes to Its Unique Appearance. *Icarus*, 123(2), 536–556. <https://doi.org/10.1006/icar.1996.0177>

[16] Liu, X., & Schmidt, J. (2020). Configuration of the Martian dust rings: shapes, densities, and size distributions from direct integrations of particle trajectories. *Monthly Notices of the Royal Astronomical Society*, 500(3), 2979–2985. <https://doi.org/10.1093/mnras/staa3084>

[17] Reuter, D. C., Simon, A. A., Hair, J., Lunsford, A., Manthripragada, S., Bly, V., Bos, B., Brambora, C., Caldwell, E., Casto, G., Dolch, Z., Finneran, P., Jennings, D., Jhabvala, M., Matson, E., Mclelland, M., Roher, W., Sullivan, T., Weigle, E., Wen, Y., Wilson, D., and Lauretta, D. S., “The OSIRIS-REx Visible and InfraRed Spectrometer (OVIRS): Spectral Maps of the Asteroid Bennu,” *Space Science Reviews*, vol. 214, Mar. 2018. <https://doi.org/10.1007/s11214-018-0482-9>

[18] “Teledyne Imaging Sensors H2RG™ Visible & Infrared Focal Plane Array,” *Teledyne Imaging Sensors*, Sep. 2017.

[19] Coradini, A., Capaccioni, F., Drossart, P., Semery, A., Arnold, G., and Schade, U., “VIRTIS: The imaging spectrometer of the Rosetta mission,” *Advances in Space Research*, vol. 24, Oct. 1998, pp. 1095–1104.

[20] “ECAM-C50,” *Malin Space Science Systems*, 2013.

[21] Bos, B. J., Ravine, M. A., Caplinger, M., Schaffner, J. A., Ladewig, J. V., Olds, R. D., Norman, C. D., Huish, D., Hughes, M., Anderson, S. K., Lorenz, D. A., May, A., Jackman, C. D., Nelson, D., Moreau, M., Kubitschek, D., Getzandanner, K., Gordon, K. E., Eberhardt, A., and Lauretta, D. S., “Touch And Go Camera System (TAGCAMS) for the OSIRIS-REx Asteroid Sample Return Mission,” *Space Science Reviews*, vol. 214, Jan. 2018. <https://doi.org/10.1007/s11214-017-0465-2>

[22] Ishiguro, M., Nakamura, R., Tholen, D. J., Hirata, N., Demura, H., Nemoto, E., Nakamura, A. M., Higuchi, Y., Sogame, A., Yamamoto, A., Kitazato, K., Yokota, Y., Kubota, T., Hashimoto, T., and Saito, J., “The Hayabusa Spacecraft Asteroid Multi-band Imaging Camera (AMICA),” *Icarus*, vol. 207, Jun. 2010, pp. 714–731. <https://doi.org/10.1016/j.icarus.2009.12.035>

[23] Cheng, A. F., Weaver, H. A., Conard, S. J., Morgan, M. F., Barnouin-Jha, O., Boldt, J. D., Cooper, K. A., Darlington, E. H., Grey, M. P., Hayes, J. R., Kosakowski, K. E., Magee, T., Rossano, E., Sampath, D., Schlemm, C., and Taylor, H. W., “Long-Range Reconnaissance Imager on New Horizons,” *Space Science Reviews*, vol. 140, Nov. 2007, pp. 189–215. <https://doi.org/10.1007/s11214-007-9271-6>

[24] Daly, M. G., Barnouin, O. S., Dickinson, C., Seabrook, J., Johnson, C. L., Cunningham, G., Haltigin, T., Gaudreau, D., Brunet, C., Aslam, I., Taylor, A., Bierhaus, E. B., Boynton, W., Nolan, M., and Lauretta, D. S., “The OSIRIS-REx Laser Altimeter (OLA) Investigation and Instrument,” *Space Science Reviews*, vol. 212, Aug. 2017, pp. 899–924. <https://doi.org/10.1007/s11214-017-0375-3>

[25] Cavanaugh, J. F., Smith, J. C., Sun, X., Bartels, A. E., Ramos-Izquierdo, L., Krebs, D. J., McGarry, J. F., Trunzo, R., Novo-Gradac, A. M., Britt, J. L., Karsh, J., Katz, R. B., Lukemire, A. T., Szymkiewicz, R., Berry, D. L., Swinski, J. P., Neumann, G. A., Zuber, M. T., and Smith, D. E., “The Mercury Laser Altimeter Instrument for the MESSENGER Mission,” *Space Science Reviews*, vol. 131, Nov. 2007, pp. 451–479. <https://doi.org/10.1007/s11214-007-9273-4>

[26] Mizuno, T., Kase, T., Shiina, T., Mita, M., Namiki, N., Senshu, H., Yamada, R., Noda, H., Kunimori, H., Hirata, N., Terui, F., and Mimasu, Y., “Development of the Laser Altimeter (LIDAR) for Hayabusa2,” *Space Science Reviews*, vol. 208, Feb. 2016, pp. 33–47. <https://doi.org/10.1007/s11214-015-0231-2>

[27] Saiki, T., Sawada, H., Okamoto, C., Yano, H., Takagi, Y., Akahoshi, Y., and Yoshikawa, M., “Small carry-on impactor of Hayabusa2 mission,” *Acta Astronautica*, vol. 84, Mar.–Apr. 2013, pp. 227–236. <https://doi.org/10.1016/j.actaastro.2012.11.010>

[28] Saiki, T., Imamura, H., Arakawa, M., Wada, K., Takagi, Y., Hayakawa, M., Shirai, K., Yano, H., and Okamoto, C., “The Small Carry-on Impactor (SCI) and the Hayabusa2 Impact Experiment,” *Space Science Reviews*, vol. 208, Oct. 2016, pp. 165–186. <https://doi.org/10.1007/s11214-016-0297-5>

- [29] Kobayashi, M., Krüger, H., Senshu, H., Wada, K., Okudaira, O., Sasaki, S., and Kimura, H., “In situ observations of dust particles in Martian dust belts using a large-sensitive-area dust sensor,” *Planetary and Space Science*, vol. 156, Jul. 2018, pp. 41–46. <https://doi.org/10.1016/j.pss.2017.12.011>
- [30] Glenn Research Center, “NASA’s Evolutionary Xenon Thruster–Commercial (NEXT–C) Fact Sheet”, 2017, <https://dart.jhuapl.edu/News-and-Resources/files/Fact-Sheet-NEXT-C.pdf>
- [31] Tooley, C.R., et al., “The Lunar Reconnaissance Orbiter Mission and Spacecraft Design,” *Space Science Review*, 2010
- [32] Glenn Research Center, “General Mission Analysis Tool (GMAT)”, <https://opensource.gsfc.nasa.gov/projects/GMAT/index.php>
- [33] Mark S. Wallace, Jeffrey S. Parker, Nathan J. Strange, and Daniel Grebow, “Orbital Operations for Phobos and Deimos Exploration”, *AIAA/AAS Astrodynamics Specialist Conference*, Aug. 2012, <https://doi.org/10.2514/6.2012-5067>
- [34] Ball Aerospace, *CT 2020 Fact Sheet*, 2020.
- [35] Aerojet Rocketdyne, In Space Propulsion Data Sheets, 2020.
- [36] Bradford Space, Fine Sun Sensor, 2021.
- [37] Spectrolab, 28.3% Ultra Triple Junction (UTJ) Solar Cells, 2008.
- [38] Caldwell, S., “State-of-the-Art of Small Spacecraft Technology,” *NASA Available:* <https://www.nasa.gov/smallsat-institute/sst-soa-2020>.
- [39] “Mars facts,” *NASA*, Available: <https://mars.nasa.gov/all-about-mars/facts/>.
- [40] Fickenor, M. M., and Dooling, D., “Multilayer insulation material guidelines,” *NASA*, Available: <https://ntrs.nasa.gov/api/citations/19990047691/downloads/19990047691.pdf>.
- [41] Hastings, L. J., Hedayat, A., and Brown, T. M., “Analytical Modeling and Test Correlation of Variable Density Multilayer Insulation for Cryogenic Storage,” *NASA*, Available: <https://ntrs.nasa.gov/api/citations/20040121015/downloads/20040121015.pdf>.
- [42] Mook, C. P., “Proceedings of conference on active temperature control - NASA technical reports server (NTRS),” *NASA Available:* <https://ntrs.nasa.gov/citations/19660023656>.
- [43] Modlin C. T., and Zipay, J. J., “The 1.5 & 1.4 Ultimate Factors of Safety for Aircraft & Spacecraft – History, Definition and Applications,” Feb. 2014, Available: <https://ntrs.nasa.gov/api/citations/20140011147/downloads/20140011147.pdf>.
- [44] Hastings, L. J., Hedayat, A., and Brown T.M., “Analytical Modeling and Test Correlation of Variable Density Multilayer Insulation for Cryogenic Storage,” *Alpha Technology and NASA Marshall Space Flight Center Huntsville*, May 2004, Available: <https://ntrs.nasa.gov/api/citations/20180001568/downloads/20180001568.pdf>.
- [45] Mallick, P.K., “Fiber-Reinforced Composites, Materials, Manufacturing, and Design, Third Edition,” *Taylor & Francis Group*, Nov. 2007
- [46] BAE Systems, RAD750® 3U CompactPCI single-board computer, 2021.
- [47] Q-Tech Corporation, Low Phase Noise Space Level OCXO, 2020 .

- [48] Bouwmeester, J., *Spacecraft Technology - Introduction to Command and Data Handling* Available: <https://ocw.tudelft.nl/wp-content/uploads/1.0-Command-and-Data-Handling-Lecture-Notes.pdf>.
- [49] Malouf, P. M., and Wallis, R. E., “The Medium-Gain Antenna of the MESSENGER Spacecraft,” *Microwave Journal*, 2005.
- [50] Vacchione, J. D., Kruid, R. C., Prata, A., Amaro, L. R., and Mittskus, A. P., “Telecommunications Antennas for the Juno Mission to Jupiter,” 2012, pp. 1–16.
- [51] Chahat, N., Amaro, L. R., Harrell, J., Wang, C., Estabrook, P., and Butman, S. A., “X-Band Choke Ring Horn Telecom Antenna for Interference Mitigation on NASA’s SWOT Mission,” *IEEE Transactions on Antennas and Propagation*, vol. 64, Jun. 2016, pp. 2075–2082.
- [52] Wertz, J. R., Larson, W. J., and D’Souza, B., eds., “Communications Architecture,” *Space Mission Analysis and Design*, El Segundo, California: Microcosm Press, 2005, pp. 533–585.
- [53] Jet Propulsion Laboratory, and Slobin, S. D., “34-m BWG Stations Telecommunications Interfaces,” Pasadena, California: Jet Propulsion Laboratory, 2015.
- [54] Jet Propulsion Laboratory, and Slobin, S. D., “Atmospheric and Environmental Effects,” Pasadena, California: Jet Propulsion Laboratory, 2015.
- [55] Taylor, J., Lee, D. K., and Shambayati, S., “Mars Reconnaissance Orbiter Telecommunications,” Pasadena, California: Jet Propulsion Laboratory, 2006.
- [56] Wertz, J. R., Larson, W. J., and D’Souza, B., eds., “Communications Architecture,” *Space Mission Analysis and Design*, El Segundo, California: Microcosm Press, 2005, pp. 562.
- [57] Bontempo, J. J., Brigeman, A. N., Fain, H. B., Gonzalez, M. C., Pinero, L. R., Birchenough, A. G., Aulizio, M. V., Fisher, J., and Ferraiuolo, B., “The NEXT-C Power Processing Unit: Lessons Learned from the Design, Build, and Test of the NEXT-C PPU for APLs DART Mission,” *AIAA Propulsion and Energy 2020 Forum*, 2020.
- [58] Wertz, J. R., Larson, W. J., and D’Souza, B., eds., “Ground Systems Design,” *Space Mission Analysis and Design*, El Segundo, California: Microcosm Press, 2005, pp. 901.
- [59] Meade, P. “New Horizons Data Management and Archiving Plan,” *Southwest Research Institute*, Available: [“https://nssdc.gsfc.nasa.gov/archive/pdmp/NHDMAP01_R2_200501.pdf”](https://nssdc.gsfc.nasa.gov/archive/pdmp/NHDMAP01_R2_200501.pdf)
- [60] Goddard Space Flight Center, Hyde, T. T., Mitchell, D. F., McCarthy, T. V., and Isaac, E. K., “General Environmental Verification Standard (GEVS) For GSFC Flight Programs and Projects”, Greenbelt, MD: Goddard Space Flight Center, 2021.
- [61] “NPD 8020.7G: Biological Contamination Control for Outbound and Inbound Planetary Spacecraft,” *NASA Science Mission Directorate*, Available: <https://nodis3.gsfc.nasa.gov/displayDir.cfm?t=NPD&c=8020&s=7G>
- [62] “NPI 8020.92 Planetary Protection Provisions for Robotic Extraterrestrial Missions,” *NASA Office of Safety and Mission Assurance*, Available: https://nodis3.gsfc.nasa.gov/OPD_docs/NID_8020_109A_.pdf
- [63] “NPR8705.4A: Risk Classification for NASA Payloads,” *NASA Office of Safety and Mission Assurance*, Available: [“https://nodis3.gsfc.nasa.gov/displayDir.cfm?t=NPR&c=8705&s=4”](https://nodis3.gsfc.nasa.gov/displayDir.cfm?t=NPR&c=8705&s=4)
- [64] Wertz, J. R., Larson, W. J., and D’Souza, B., eds., “Risk and Reliability,” *Space Mission Analysis and Design*, El Segundo, California: Microcosm Press, 2005, pp. 772.
- [65] Wertz, J. R., Larson, W. J., and D’Souza, B., eds., “Cost Estimating,” *Space Mission Analysis and Design*, El Segundo, California: Microcosm Press, 2005, pp. 298-299.

[66] Wertz, J. R., Larson, W. J., and D'Souza, B., eds., “Cost Estimating,” *Space Mission Analysis and Design*, El Segundo, California: Microcosm Press, 2005, pp. 303.

[67] Wertz, J. R., Larson, W. J., and D'Souza, B., eds., “Cost Estimating,” *Space Mission Analysis and Design*, El Segundo, California: Microcosm Press, 2005, pp. 309.

[68] Hofer, R. R., and Randolph, T. M., “Mass and Cost Model for Selecting Thruster Size in Electric Propulsion Systems,” *Journal of Propulsion and Power*, vol. 29, Feb. 2013, pp. 166–177.

[69] Wertz, J. R., Larson, W. J., and D'Souza, B., eds., “Cost Estimating,” *Space Mission Analysis and Design*, El Segundo, California: Microcosm Press, 2005, pp. 318.

[70] Wertz, J. R., Larson, W. J., and D'Souza, B., eds., “Cost Estimating,” *Space Mission Analysis and Design*, El Segundo, California: Microcosm Press, 2005, pp. 319.